Nordman H, Pavlenko V P and Weiland J 1993 *Phys. Plasmas* B **5** 402
Knobloch E and Weiss N O J 1983 *Physica* D **9** 379 (see also Bekki N and Karakisawa T 1995 *Phys. Plasmas* **2** 2945)
[4.17] Itoh K, Itoh S-I and Fukuyama A 1992 *Phys. Rev. Lett.* **69** 1050
Itoh K, Itoh S-I, Fukuyama A, Yagi M and Azumi M 1994 *Plasma Phys. Control. Fusion* **36** 279
[4.18] Tange T, Inoue S, Itoh K and Nishikawa K 1979 *J. Phys. Soc. Japan* **46** 266
[4.19] Fried B D and Conte S D 1961 *The Plasma Dispersion Function* (New York: Academic)

K Itoh, S-I Itoh, A Fukuyama
"Transport and structural formation in plasmas"
IOP, 1999

Chapter 5

Low Frequency Modes in Confined Plasmas

In this chapter, typical examples of low frequency modes in plasmas are explained. The mechanisms to determine the dispersion relation are described.

5.1 Modes and Dispersion Relations

Fluctuations in plasmas do not form a white noise, but oscillatory patterns are often excited. The spatio-temporal patterns that appear (either stationary or propagating) are called *modes*. The spectrum of mode is a characterizing information in the continuous media. If one imposes an external perturbation of the form

$$\tilde{\boldsymbol{E}}_{ext} \exp(\mathrm{i}\boldsymbol{k} \cdot \boldsymbol{x} - \mathrm{i}\omega t)$$

(where $\boldsymbol{k}$, ω can be complex), then the charged elements of plasma are displaced so as to generate a response field

$$\tilde{\boldsymbol{E}}_{induced} \exp(\mathrm{i}\boldsymbol{k} \cdot \boldsymbol{x} - \mathrm{i}\omega t).$$

If there is a relation of $(\boldsymbol{k}, \omega)$

$$\omega = \omega(\boldsymbol{k}) \tag{5.1}$$

for which the ratio $\tilde{E}_{induced}/\tilde{E}_{ext}$ becomes very large, then a pattern $\exp\{\mathrm{i}\boldsymbol{k} \cdot \boldsymbol{x} - \mathrm{i}\omega(\boldsymbol{k})t\}$ is expected to have a large amplitude and to be selectively observed. Such a pattern is called a *mode*, and the relation (5.1) is called the dispersion relation.

The search of various modes in confined plasmas is a fundamental task in investigating the fluctuations and transport in plasmas. The parameters $(\boldsymbol{k}, \omega)$ are related to the spatial-temporal scales that play roles in the transport processes.

The dispersion relation is determined by the electric conductivity tensor in equation (4.39), $\tilde{\boldsymbol{J}}_{k\omega} = (\sum_j \sigma_{j.k\omega})\tilde{\boldsymbol{E}}_{k\omega}$. The dielectric tensor is introduced (according to the convention) as

$$\varepsilon(k,\omega) = \boldsymbol{I} - \frac{\mathrm{i}c^2\mu_0}{\omega}\left(\sum_j \sigma_{j.k\omega}\right) \tag{5.2}$$

where $\boldsymbol{I}$ is the unit tensor, μ_0 is the magnetic permeability of vacuum and c is the velocity of light. Substituting equation (4.39) into Maxwell's equation one has the relation

$$\left[\varepsilon(k,\omega) - \left(\frac{kc}{\omega}\right)^2\left(\boldsymbol{I} - \frac{\boldsymbol{kk}}{k^2}\right)\right]\boldsymbol{E}_{k.\omega} = \frac{c\mu_0}{\mathrm{i}\omega}\boldsymbol{j}_{ext;k.\omega} \tag{5.3}$$

where $\boldsymbol{j}_{ext;k.\omega}$ is an externally imposed current perturbation of the Fourier component $(\boldsymbol{k}, \omega)$. Equation (5.3) predicts that the perturbed field $\boldsymbol{E}_{k.\omega}$ can take a finite amplitude even without the external perturbation, if the condition

$$\det\left|\varepsilon(\boldsymbol{k},\omega) - \left(\frac{kc}{\omega}\right)^2\left(\boldsymbol{I} - \frac{\boldsymbol{kk}}{k^2}\right)\right| = 0 \tag{5.4}$$

is satisfied. Equation (5.4) is the condition that $\boldsymbol{E}_{k.\omega}$ has a nontrivial solution for $\boldsymbol{j}_{ext;k.\omega} = 0$. The dispersion relation (5.1) is given as a solution of equation (5.4).

The relation (5.1) could depend on the amplitude of perturbations: if it is dependent, it is a *nonlinear dispersion relation*. In the zero-amplitude limit of perturbations, equation (5.1) is the *linear* dispersion relation. The literature explains the various linear modes in plasmas in detail (e.g. [2.1–2.6]). Among various modes in plasmas, those of low frequencies have particular importance in the study of plasma transport. This is because the radial excursion of plasma elements is larger if the frequency is lower, for given amplitude of perturbations, as is shown in equation (4.7). In addition to this, fluctuations which are relevant to the transport are often excited by the plasma inhomogeneities.

5.1.1 Fluid Equations

The response of the plasma to a perturbed field is calculated based on the continuity equation, equation of motion and energy balance equation (equation of state). In the fluid description of the plasma, they are given as [2.3, 2.4]

$$\frac{\partial}{\partial t}n_j + \nabla\cdot(n_j\boldsymbol{V}_j) = 0 \tag{5.5}$$

$$m_j n_j \frac{\mathrm{d}}{\mathrm{d}t}\boldsymbol{V}_j = e_j n_j(\boldsymbol{E} + \boldsymbol{V}_j\times\boldsymbol{B}) - \nabla p_j - \nabla\cdot\boldsymbol{\Pi}_j \tag{5.6}$$

and

$$\frac{3}{2}n_j\frac{\partial}{\partial t}T_j + p_j\nabla\cdot\boldsymbol{V}_j = -\nabla\cdot\boldsymbol{q}_j - \boldsymbol{\Pi}_j\nabla\boldsymbol{V}_j + P_j \tag{5.7}$$

where

$$\frac{\mathrm{d}}{\mathrm{d}t} = \frac{\partial}{\partial t} + \boldsymbol{V}\cdot\nabla \tag{5.8}$$

is the total time derivative, $\boldsymbol{q}_j$ is the heat flux, $\boldsymbol{\Pi}_j$ is the viscous tensor and P_j is the energy input. The off-diagonal tensor $\boldsymbol{\Pi}$ vanishes for the case of an isotropic velocity distribution. The energy input includes the energy exchange between plasma species.

The set of equations requires the knowledge on the energy transport and deformation of the distribution function; it is *not* closed in the realm of a fluid description, but needs the kinetic analysis of the plasma response. In some cases, however, a relevant and simplified expression is obtained, and is called the *equation of state*. If the temporal change is fast in comparison with the flow rate of the energy, then the adiabatic condition

$$\frac{\mathrm{d}}{\mathrm{d}t}(p_j n_j^{-\gamma}) = 0 \tag{5.9}$$

is a good approximate relation to close the set of equations. The parameter γ in this equation is the specific heat ratio. In contrast, if the energy equilibration is faster, then the simplification

$$T_j = \text{constant} \tag{5.10}$$

is a good approximation.

These equations (5.5)–(5.7) and (5.9) (or (5.10)) describe the plasma dynamics combined with Maxwell's equation below

$$\nabla\times\boldsymbol{B} = \mu_0\left(\sum_j \boldsymbol{J}_j + \varepsilon_0\frac{\partial}{\partial t}\boldsymbol{E}\right) \tag{5.11}$$

$$\nabla\times\boldsymbol{E} = -\frac{\partial}{\partial t}\boldsymbol{B}. \tag{5.12}$$

5.1.2 Linearization

The evolution of perturbations is studied by the expansion of plasma parameters as

$$n = n_0 + \tilde{n} \qquad \boldsymbol{V} = \boldsymbol{V}_0 + \tilde{\boldsymbol{V}} \qquad p = p_0 + \tilde{p} \tag{5.13}$$

in the vicinity of equilibrium parameters. (Here 'equilibrium' refers to the stationary mechanical equilibrium, and is denoted by the suffix 0. The suffix j, distinguishing plasma species, is suppressed if not confused.) Terms are retained up to the first order of perturbation. The equation of motion and the continuity equation, for perturbed components, are given as

$$mn\left(\frac{\partial}{\partial t}\tilde{\boldsymbol{V}} + \boldsymbol{V}_0\cdot\nabla\tilde{\boldsymbol{V}} + \tilde{\boldsymbol{V}}\cdot\nabla\boldsymbol{V}_0\right) = en(\tilde{\boldsymbol{E}} + \boldsymbol{V}_0\times\tilde{\boldsymbol{B}} + \tilde{\boldsymbol{V}}\times\boldsymbol{B}_0) - \nabla\tilde{p} \tag{5.14}$$

$$\frac{\partial}{\partial t}\tilde{n} + \nabla \cdot (\tilde{n}V_0 + n_0\tilde{V}) = 0. \tag{5.15}$$

With the help of the equation of state, one obtains either

$$\frac{\partial}{\partial t}\tilde{p}n_0^{-\gamma} - \gamma p_0 n_0^{-\gamma-1}\frac{\partial}{\partial t}\tilde{n} + \tilde{V} \cdot \nabla(p_0 n_0^{-\gamma}) = 0 \qquad \text{(adiabatic limit)} \tag{5.16}$$

or

$$\tilde{T} = 0 \qquad \text{(iso-thermal limit)}. \tag{5.17}$$

The perturbed density, velocity and temperature (or pressure) ($\tilde{n}_j$, $\tilde{V}_j$, $\tilde{T}_j$) are calculated in terms of the perturbed electromagnetic fields ($\tilde{\boldsymbol{E}}$, $\tilde{\boldsymbol{B}}$).

5.1.3 Model Picture of Plasmas

A basic approximation in the plasma response to a low frequency perturbation is as follows. Namely,

(i) electrons can almost freely move along the field line, or
(ii) the parallel electric conductivity is high,

characterizing the *high-temperature* plasmas. The magnetic field is strong, i.e.,

(iii) the magnetic pressure $B^2/2\mu_0$ is much higher than the plasma pressure p.

The ratio of the plasma pressure to the magnetic pressure is called the 'plasma beta-value'. It is conventionally expressed as

$$\beta \equiv \frac{2\mu_0 p}{B^2} \tag{5.18}$$

and is considered to be much smaller than unity here. The condition

(iv) the scale-length is much longer than the Debye length, $k\lambda_D \ll 1$,

is often employed.

5.2 Sound Wave and Shear Alfvén Wave

When a perturbation amplitude is small, and a linear response of a plasma is of interest, then a calculation of the dielectric tensor follows a well defined procedure. We leave the detailed analysis of linear response functions in literature (e.g., [2.1–2.8]) and here explain two examples of the low frequency modes in magnetized plasmas, the *sound mode* and the *shear Alfvén mode*. These two branches of waves are defined in a uniform plasma and are modified in various ways in non-uniform plasmas. The sound mode and the shear Alfvén mode constitute the basis for understanding the fluctuations in confined plasmas.

A uniform, stationary and slab (planar) plasma is considered (figure 5.1). Influences of nonuniformity are discussed in the following sections.

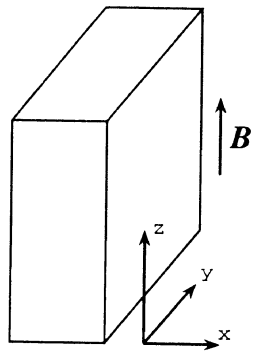

Figure 5.1. Slab plasma model with strong magnetic field.

5.2.1 Ion Sound Wave

Let us consider a perturbation that is propagating in the direction of magnetic field,

$$\boldsymbol{k} = (0, 0, k_\parallel). \tag{5.19}$$

(The propagation in the direction of the magnetic field is not an essential feature of the ion sound wave. This choice is made just for simplicity.) In terms of the fluid description, equilibrium plasma parameters (n_0, T_0) are constant and the plasma is staying still, $V_0 = 0$. In this circumstance, a response to an electrostatic perturbation,

$$\tilde{\boldsymbol{E}} = -\nabla\tilde{\phi}$$

is studied. The relevant mode is in the range

$$|k_\parallel v_{thi}| \ll \omega \ll |k_\parallel v_{the}| \tag{5.20}$$

where v_{thi} and v_{the} are thermal velocities of ions and electrons, respectively. The ion response is approximated as adiabatic. The electron response is iso-thermal, because the phase velocity $\omega/k_\parallel$ is slower than the thermal velocity v_{the}.

The equation of motion for ions is written as

$$-\mathrm{i}m_i n_i \omega \tilde{V}_{i,z} = -\mathrm{i}k_\parallel e_i n_i \tilde{\phi} - \mathrm{i}k_\parallel \tilde{p}_i. \tag{5.21}$$

The continuity equation yields the relation

$$-\mathrm{i}\omega\tilde{n}_i + \mathrm{i}k_\parallel n_0 \tilde{V}_{i,z} = 0. \tag{5.22}$$

If the adiabatic relation is used for ions, the equation of state (5.9) yields $\tilde{p}_i = \gamma_i T_i \tilde{n}_i$. Eliminating $\tilde{V}_i$ and $\tilde{p}_i$ from equations (5.21) and (5.22) with

the help of the adiabatic condition, one has

$$\frac{\tilde{n}_i}{n_i} = \frac{Z_i T_e k_\parallel^2}{m_i \omega^2} \frac{1}{1 - \gamma_i k_\parallel^2 v_{thi}^2 \omega^{-2}} \frac{e\tilde{\phi}}{T_e} \tag{5.23}$$

where Z_i is the charge number of ions, $e_i = Z_i e$.

Because the electron mass is small, the equation of motion for electrons gives an approximate relation as

$$-en_e \tilde{E}_z - \mathrm{i} k_\parallel \tilde{p}_e \cong 0.$$

The fast motion of electrons tends to equilibrate the temperature along the field line, so that an iso-thermal approximation, $\tilde{T}_e \simeq 0$, is used. With the help of equation (5.17), the electron density is given as

$$\frac{\tilde{n}_e}{n_e} = \frac{e\tilde{\phi}}{T_e}. \tag{5.24}$$

The Poisson equation is written in the form of a charge neutrality condition, i.e.,

$$\tilde{n}_e \cong Z_i \tilde{n}_i. \tag{5.25}$$

Substituting the responses (5.23) and (5.24) into equation (5.25), the dispersion relation is finally given as

$$\omega^2 = c_s^2 k_\parallel^2 \tag{5.26-1}$$

with

$$c_s^2 = \frac{(Z_i T_{e0} + \gamma_i T_{0i})}{m_i}. \tag{5.26-2}$$

The dispersion relation (5.26), shown in figure 5.2, indicates that this perturbation propagates with a constant phase velocity,

$$|\omega / k_\parallel| = c_s$$

which is called the ion sound velocity.

This ion sound mode is similar to sound waves in a neutral gas. Note that the ion sound speed is finite in the limit of

$$T_{i,0} \to 0.$$

An expansion of ions in a condensed layer to a rarefied layer is governed by the electric field, not only by the pressure of ions. This is in contrast to a sound wave in neutral gas, where the expansion is governed by the pressure. The ion sound mode in plasmas has a collective nature, where plasma particles in different locations are interacting with each other through the long range electric field. Free electron motions along a field line, given in equation (5.24), play an essential role in determining the pattern of compression or decompression of ions.

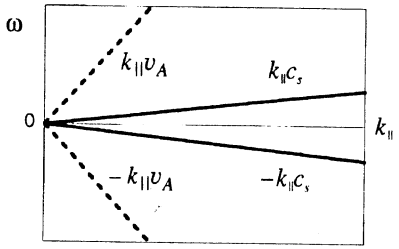

Figure 5.2. Dispersion relation of the ion sound wave (solid line) and the shear Alfvén wave (dashed line).

5.2.2 Shear Alfvén Wave

A nearly free electron motion along the field line gives another type of mode in a magnetized plasma. The magnetic perturbation can also propagate in a plasma as a mode. The *shear Alfvén mode* is accompanied by the perturbed magnetic field in the direction perpendicular to a main magnetic field, $\tilde{B}_\perp$. (There is another type of perturbation, which is associated with the magnetic perturbation in the direction of the main magnetic field, $\tilde{B}_\parallel$. For such a mode, a perturbation of magnetic energy associated with the wave is large. The excitation of such a mode requires the larger free energy.)

For an electromagnetic perturbation, the response in a plasma to induce a perturbed current is a key. We consider a perturbation which propagates in the z-direction, equation (5.19), with the component

$$\tilde{\boldsymbol{B}} = (\tilde{B}_x, 0, 0) \tag{5.27}$$

$$\tilde{\boldsymbol{E}} = \left(0, -\frac{\omega}{k_\parallel}\tilde{B}_x, 0\right). \tag{5.28}$$

In expressing the electric field perturbation $\tilde{E}_y$ in terms of the magnetic perturbation, $\tilde{B}_x$, we use equation (5.12).

Summing up equation (5.14) for electrons and ions, and subtracting one from the other, one has the MHD equations. Components in the direction perpendicular to the magnetic field are of interest,

$$m_i n_i \frac{\partial}{\partial t}\tilde{\boldsymbol{V}} = \tilde{\boldsymbol{J}} \times \boldsymbol{B}_0 - \nabla \tilde{p} \tag{5.29}$$

$$\tilde{E}_y + (\tilde{\boldsymbol{V}} \times \boldsymbol{B}_0)_y - \frac{1}{en}\nabla_y \tilde{p}_i = 0. \tag{5.30}$$

In the calculation of equation (5.30), the ion inertia effect is neglected since the change rate is slow in time compared to the ion cyclotron frequency. The

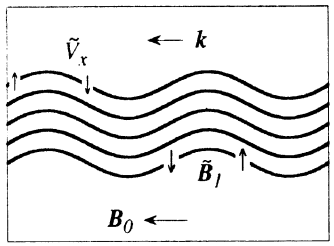

Figure 5.3. Flow and distorted magnetic field line for the propagation of a shear Alfvén wave.

electron inertia effect is also neglected. In this simplified approximation, a friction on electrons by ions is also neglected. These equations are often called the *ideal MHD equation*. For perturbations of the form of equation (5.19), equations (5.29) and (5.30) provide the relation

$$\tilde{V}_x = B_0^{-1}\tilde{E}_y \tag{5.31}$$

and

$$\tilde{J}_y = -\frac{\mathrm{i}m_i n_i \omega}{B_0^2}\tilde{E}_y = \frac{\mathrm{i}m_i n_i \omega^2}{B_0^2 k_\parallel}\tilde{B}_x. \tag{5.32}$$

Substituting equation (5.32) into Maxwell's equation,

$$\tilde{B}_x = -\frac{\mathrm{i}\mu_0}{k_\parallel}\tilde{J}_y \tag{5.33}$$

one has the dispersion relation

$$\omega^2 = k_\parallel^2 v_A^2 \tag{5.34}$$

with

$$v_A^2 = \frac{B_0^2}{m_i n_i \mu_0} \tag{5.35}$$

where v_A is called the Alfvén velocity. The dispersion relation is plotted in figure 5.2.

The patterns of current, displacement and perturbed field are shown in figure 5.3. The plasma motion, equation (5.31), is expressed as

$$\tilde{V}_x = (\tilde{B}_x/B_0)v_A.$$

This shows that the plasma motion satisfies the frozen-in condition, i.e., the distortion of the magnetic field lines coincides with the displacement of the plasma. The frozen-in condition follows from Ohm's law equation (5.30), and is satisfied generally so long as the parallel resistance is not important.

An approximately free electron motion along the field line is essential in determining the mode structures of both the ion sound mode and the Alfvén mode. The 'free' parallel motion of electrons is an idealization. In reality, however, the free electron motion is just an approximation, and a small but finite impedance affects an idealized 'free' electron motion. This impedance governs the dynamics of such modes as is explained in the next chapter.

5.3 Drift Wave and Drift-Alfvén Wave

5.3.1 Diamagnetic Drift

When a plasma is inhomogeneous, as is illustrated in figure 5.4, there appears a preferential direction for a wave. The force balance of a plasma implies that there is a current, i.e., the difference of flow velocities of ions and electrons, on the magnetic surface. A current which flows perpendicular to a magnetic field line is called a diamagnetic current. (A current in the direction of the magnetic field is called a force-free current, because it does not give rise to the Lorentz force.) The flow velocity of a plasma in the $\nabla p \times \boldsymbol{B}$-direction is named a diamagnetic velocity. It is given in the presence of the density gradient as

$$\boldsymbol{V}_d = \frac{T_j}{e_j B}\frac{1}{n_j}\frac{\mathrm{d}n_j}{\mathrm{d}x}\hat{y} \tag{5.36}$$

in the configuration of figure 5.4. It is seen that the diamagnetic current, $\boldsymbol{J}_d = (e_i n_i V_{di} - e n_e V_{de})\hat{\boldsymbol{y}}$, satisfies the force balance equation, $\boldsymbol{J}_d \times \boldsymbol{B} = \nabla p$, equation (3.1). A similar diamagnetic flow is generated by the temperature gradient as well.

In a microscopic picture, the flow equation (5.36) is generated by the difference of the number density of gyrating (i.e., cyclotron motion) particles (figure 5.5(a)). In a small volume of interest at location x, ions which move in the y-direction have the gyro-centre at the position with larger x, $x' = x + \rho_i$. Ions moving in the $-y$-direction have the centre at the position with smaller x, $x' = x - \rho_i$. Because of the density gradient in the x-direction, the number of particles moving in the $-y$-direction is larger. As a result of this difference, the fluid velocity results in the $-y$-direction.

In contrast, the drift due to an inhomogeneity of magnetic field causes motion of the gyro-centre of the particles in the drift direction (in the direction of $\nabla B \times \boldsymbol{B}$). Figure 5.5(b) illustrates the case of inhomogeneous magnetic field; a field is mainly directed in the z-direction, but its magnitude gradually increases in the x-direction. Due to the small change of magnetic field across the cyclotron radius, a cyclotron orbit does not close itself on the x–y-plane, and a resultant drift in the y-direction appears. The drift velocity due to the

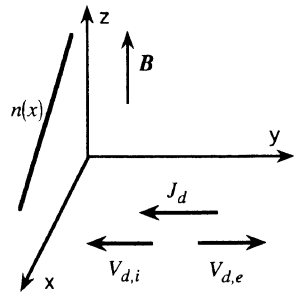

Figure 5.4. Diamagnetic flow V_d and diamagnetic current J_d in an inhomogeneous plasma.

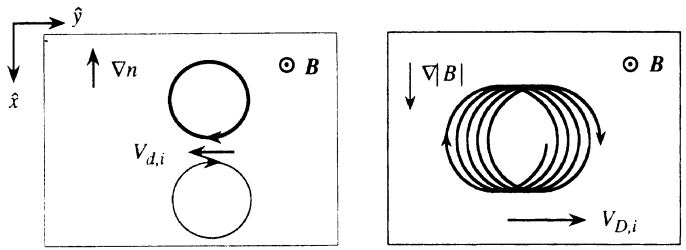

Figure 5.5. Gyro-motion and diamagnetic flow of ions in inhomogeneous plasma (a). Configuration of the plasma is the same as figure 5.4. If the magnetic field strength is varying in the x-direction, flow in the y-direction V_D also appears (b).

magnetic field inhomogeneity, $V_{D.j}$, is given as

$$\boldsymbol{V}_{D.j} = \frac{W_j}{e_j B}\left(\frac{1}{|B|}\frac{\mathrm{d}|B|}{\mathrm{d}x}\right)\hat{y} \tag{5.37}$$

where W_j is the energy of particles. The diamagnetic drift and the magnetic curvature drift are in the same direction (additive) if the condition

$$\nabla p \cdot \nabla|B| > 0 \tag{5.38}$$

holds.

As is shown in the next chapters, the sign of the product $\nabla p \cdot \nabla|B|$ is important for the developments of fluctuations in inhomogeneous plasmas. The case of equation (5.38) is called *bad curvature*. (Good curvature if $\nabla p \cdot \nabla|B| < 0$.) The name 'curvature' is used because the magnetic field strength becomes inhomogeneous when the magnetic field line is slightly curved. For a vacuum magnetic field, the scale-length of curvature and the inhomogeneity scale-length of field strength are equal (see also subsection 6.2.1).

5.3.2 Drift Wave

When the drift velocity is not negligible in comparison with the phase velocity, a preferential direction appears in a wave propagation. Consider an electrostatic perturbation, which is obliquely propagating,

$$\boldsymbol{k} = (0, k_y, k_\parallel). \tag{5.39}$$

The electric field is expressed in terms of the perturbed potential as

$$\tilde{\boldsymbol{E}} = -\mathrm{i}\boldsymbol{k}\tilde{\phi}. \tag{5.40}$$

In an inhomogeneous plasma, a new term appears in the continuity equation, equation (5.22), as

$$-\mathrm{i}\omega\tilde{n}_i + \mathrm{i}k_\parallel n_{i0}\tilde{V}_{iz} + \tilde{V}_{i.x}\frac{\mathrm{d}n_{i0}}{\mathrm{d}x} = 0 \tag{5.41}$$

with

$$\tilde{V}_{i.x} = -\mathrm{i}k_y\tilde{\phi}/B.$$

(One may expect that a Doppler shift term like $\mathrm{i}k_y V_{di}$ would appear in the time derivative, e.g., $\mathrm{i}k_y V_{di}\tilde{n}_i$ in the left-hand side of equation (5.41). However, this is not the case. Recall that particles do not move in the direction of the diamagnetic drift, as is explained in relation with figure 5.5(a) [1.6].) The equation of ion motion in the z-direction is unchanged and equation (5.21) gives a relation

$$\tilde{V}_{i.z} = k_\parallel m_i^{-1}\omega^{-1}(e_i\tilde{\phi} + n_{i0}^{-1}\gamma_i T_{i0}\tilde{n}_i) \tag{5.42}$$

with the equation of state, equation (5.9). Substituting perturbed velocities $\tilde{V}_{i.x}$ and $\tilde{V}_{i.z}$ into equation (5.41), one finds the perturbed ion density as

$$\frac{\tilde{n}_i}{n_{i0}} = \left(\omega - \frac{k_\parallel^2}{\omega m_i}\gamma_i T_{i0}\right)^{-1}\left(\frac{k_\parallel^2 T_i}{\omega m_i} - \frac{k_y T_i}{e_i B n_{i0}}\frac{\mathrm{d}n_{i0}}{\mathrm{d}x}\right)\frac{e_i\tilde{\phi}}{T_i}. \tag{5.43}$$

The free motion of electrons gives the Boltzmann relation for the electron response as equation (5.24), $\tilde{n}_e/n_e = e\tilde{\phi}/T_e$. Substitution of equations (5.24) and (5.43) into the charge neutrality condition $e_i\tilde{n}_i = e\tilde{n}_e$ gives the dispersion relation as

$$\omega^2 - \omega\omega_* - k_\parallel^2 c_s^2 = 0 \tag{5.44}$$

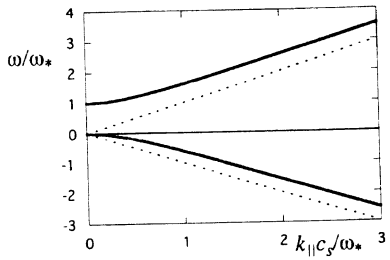

Figure 5.6. Dispersion relation for the electrostatic drift wave.

where ω_* is the drift frequency defined by

$$\omega_* = k_y V_{de} = -\frac{k_y T_e}{eBn_0}\frac{\mathrm{d}n_0}{\mathrm{d}x}. \tag{5.45}$$

The dispersion relation is shown in figure 5.6.

When the mode propagates nearly perpendicular to the magnetic field line, $k_y^2 V_{de}^2 \gg k_\parallel^2 c_s^2$, i.e.,

$$|k_y|\frac{\rho_s}{L_n} > |k_\parallel| \tag{5.46}$$

the frequency of the mode is approximately given as

$$\omega = \omega_*. \tag{5.47}$$

In equation (5.46) L_n is the scale-length of the density gradient,

$$-\nabla n/n = (1/L_n)\hat{x}$$

and ρ_s is the ion cyclotron radius evaluated by the electron temperature.

If the wave propagates mainly in the z-direction, $k_y \to 0$, the dispersion relation reduces to that of an ion sound wave.

5.3.3 Drift-Alfvén Wave

The electromagnetic mode is also influenced by an inhomogeneity. A preferential direction of propagation is chosen as equation (5.39), $\boldsymbol{k} = (0, k_y, k_\parallel)$. The perturbed magnetic field is in the x-direction, like equation (5.28), but couples with E_z due to the oblique propagation. The perturbed field is expressed as

$$\tilde{\boldsymbol{B}} = (\tilde{B}_x, 0, 0) \tag{5.48}$$

$$\tilde{\boldsymbol{E}} = (0, \tilde{E}_y, \tilde{E}_z). \tag{5.49}$$

Perturbations of magnetic and electric fields are related to each other, and are expressed as

$$\tilde{B}_x = \frac{1}{\omega}(k_y \tilde{E}_z - k_\parallel \tilde{E}_y) \tag{5.50}$$

by use of Maxwell's equation.

Plasma responses are calculated as in the preceding section. The calculation is straightforward, but a little lengthy. The explicit derivation is shown in appendix 5A. The perturbed current in the z-direction is obtained as

$$\tilde{J}_z = \frac{\mathrm{i}m_i n_{i0}}{B^2}\frac{(\omega + |\omega_{*i}|)k_y}{k_\parallel}\tilde{E}_y \tag{5.51}$$

where ω_{*i} is the ion-drift frequency,

$$\omega_{*i} = -\frac{T_i}{T_e}\omega_*. \tag{5.52}$$

Ampère's law, $\partial \tilde{B}_x/\partial y = \mu_0 \tilde{J}_z$, combines the magnetic and electric perturbations as

$$\tilde{B}_x = -\frac{(\omega + |\omega_{*i}|)}{k_\parallel v_A^2}\tilde{E}_y. \tag{5.53}$$

This relation shows that the magnetic component becomes noticeable if the phase velocity is in the range of Alfvén velocity, $|\omega/k_\parallel v_A| > 1$. The dispersion relation is given as

$$\omega^2 - \omega\omega_* - k_\parallel^2 c_s^2 = \frac{\omega^2(\omega - \omega_*)(\omega + |\omega_{*i}|)}{k_\parallel^2 v_A^2}. \tag{5.54}$$

Equation (5.54) describes drift branches (5.43) and the electromagnetic branches. In the electrostatic limit, $|\omega/k_\parallel v_A| \ll 1$, equation (5.54) reproduces the dispersion relation of the electrostatic drift waves. In an opposite limit, $|\omega/k_\parallel v_A| > 1$, it provides the drift-Alfvén mode. In the limit of $|\omega/k_\parallel v_A| > 1$, the relation $|\omega/k_\parallel c_s| \gg 1$ holds, because the sound speed is much smaller than the Alfvén velocity for the parameter of our interest, $\beta \ll 1$. Neglecting the $k_\parallel^2 c_s^2$ term in the left-hand side, one simplifies equation (5.54) as

$$(\omega - \omega_*)(\omega^2 + \omega|\omega_{*i}| - k^2 v_A^2) = 0. \tag{5.55}$$

In addition to the drift wave, $\omega \simeq \omega_*$, two other modes are obtained. The electromagnetic branch, in the small $k_\parallel$ limit, becomes the mode propagating in the direction of the ion diamagnetic drift,

$$\omega = -\frac{T_i}{T_e}\omega_*. \tag{5.56}$$

In a large $k_\parallel$ limit, $|k_\parallel| v_A \gg \omega_*$, the shear Alfvén wave is recovered. The dispersion relation, which is obtained from equation (5.54), is illustrated in figure 5.7.

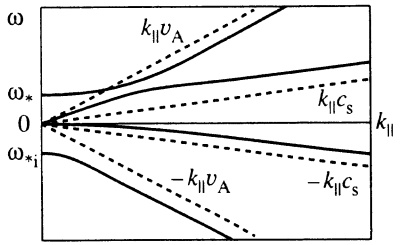

Figure 5.7. Dispersion relation for the drift wave and drift-Alfvén wave.

Appendix 5A Drift-Alfvén Wave

Equation of motion for electrons in the z-direction is given as

$$-i\omega m_e n_e \tilde{V}_{e,z} = -en_e\tilde{E}_\parallel - ik_\parallel T_e\tilde{n}_e + en_e V_{de}\tilde{B}_x. \tag{5A.1}$$

Neglecting the electron mass, we have

$$\frac{\tilde{n}_e}{n_e} = \frac{ie\tilde{E}_\parallel}{k_\parallel T_e} - iV_{de}\frac{e\tilde{B}_x}{k_\parallel T_e}. \tag{5A.2}$$

The magnetic perturbation appears through the Lorentz force.

The equation of motion for ions in the z-direction is expressed as

$$-i\omega m_i n_i \tilde{V}_{i,z} = e_i n_i \tilde{E}_\parallel - ik_\parallel \gamma_i T_i \tilde{n}_i + e_i n_i V_{di}\tilde{B}_x. \tag{5A.3}$$

The perturbed perpendicular velocity of ions is given as

$$\tilde{V}_{i,x} = \frac{\bar{\tilde{E}}_y}{B} - \frac{ik_y\gamma_i T_i}{eB}\frac{\tilde{n}_i}{n_i} \tag{5A.4}$$

$$\tilde{V}_{i,y} = -\frac{im_i\omega}{eB^2}\bar{\tilde{E}}_y - \frac{m_i\omega k_y\gamma_i T_i}{e^2B^2}\frac{\tilde{n}_i}{n_i}. \tag{5A.5}$$

In this expression $\bar{\tilde{E}}_y$ indicates the electric field, which is averaged over the gyro-motion of ions. (See figure 5A.1.) It is given as

$$\bar{\tilde{E}}_y \simeq (1 - k_y^2\rho_i^2)\tilde{E}_y. \tag{5A.6}$$

The $\boldsymbol{E} \times \boldsymbol{B}$ velocity is nearly equal for ions and electrons. Owing to the larger gyro-orbit for ions, the effective electric field acting on ions is smaller than that on electrons.

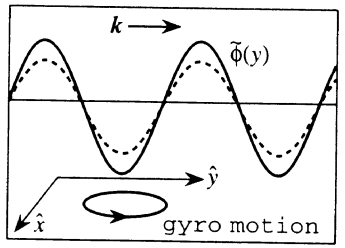

Figure 5A.1. Ions feel an averaged field (dashed line) owing to the gyro-motion. The effective field is weaker than the real field (solid line).

The ion response is calculated by substituting equations (5A.3), (5A.4) and (5A.5) into the continuity equation as

$$\frac{\tilde{n}_i}{n_{i0}} = \left(\omega - \frac{k_\parallel^2}{\omega m_i}\gamma_i T_{i0}\right)^{-1}\left[(\omega_* - \omega k_y^2\rho_i^2)\frac{ie\bar{\tilde{E}}_y}{k_y T_e} + \frac{k_\parallel^2 T_e}{\omega m_i}\frac{ie\tilde{E}_z}{k_\parallel T_e} - \frac{iek_\parallel V_{di}}{\omega m_i}\tilde{B}_x\right]. \tag{5A.7}$$

Keeping the first order correction of the finite-gyro-radius effect, $k_y^2\rho_i^2 \ll 1$, we obtain the ion density perturbation as

$$\frac{\tilde{n}_i}{n_{i0}} = \left(\omega - \frac{k_\parallel^2}{\omega m_i}\gamma_i T_{i0}\right)^{-1} \times \left[(\omega_* - (\omega + \omega_*)k_y^2\rho_i^2)\frac{ie\tilde{E}_y}{k_y T_e} + \frac{k_\parallel^2 T_e}{\omega m_i}\frac{ie\tilde{E}_z}{k_\parallel T_e} - \frac{iek_\parallel V_{di}}{\omega m_i}\tilde{B}_x\right]. \tag{5A.8}$$

In the electrostatic limit, this is reduced to equation (5.41) if the finite-gyro-radius effect is neglected.

The charge neutrality condition, $\tilde{n}_e/n_e = \tilde{n}_i/n_i$, with equations (5A.2) and (5A.3), gives the relation as

$$\left\{\omega - \omega_* - \frac{k_\parallel^2 c_s^2}{\omega} + (\omega + \omega_*)k_\perp^2\rho_i^2\right\}\frac{ie\tilde{E}_y}{k_y T_e} = -\omega\left\{\omega - \omega_* + (\omega_* - |\omega_{*i}| - \omega)\frac{k_\parallel^2 c_s^2}{\omega^2}\right\}\frac{ie\omega\tilde{B}_x}{T_e k_y k_\parallel}. \tag{5A.9}$$

In a derivation of equation (5A.9), $\tilde{E}_z$ is expressed in terms of $\tilde{E}_y$ and $\tilde{B}_x$ by use of equation (5.50).

The ratio of the magnetic perturbation to the electric perturbation is given from Ampère's law. The perturbed current is calculated as

$$\nabla_{\parallel} \cdot \tilde{J}_z = -\nabla_{\perp} \cdot \{en_0(V_{i,x} - V_{e,x})\hat{x} + en_0(V_{i,y} - V_{e,y})\hat{y}\}. \tag{5A.10}$$

The divergence of net current vanishes, because the charge neutrality condition holds. Owing to the finite-gyro-radius effect, the divergence of the current in the x-direction remains as

$$\nabla_{\perp} \cdot \{en_0(V_{i,x} - V_{e,x})\hat{x}\} = -e\frac{dn_0}{dx}k_y^2\rho_i^2\frac{\tilde{E}_y}{B}. \tag{5A.11}$$

The divergence of the perturbed diamagnetic current is given as

$$\nabla_{\perp} \cdot \{en_0(V_{i,y} - V_{e,y})\hat{y}\} = \frac{m_i n_i k_y \omega}{B^2}\tilde{E}_y. \tag{5A.12}$$

Substitution of equations (5A.11) and (5A.12) into equation (5A.10) gives the parallel current as

$$\tilde{J}_z = \frac{m_i n_i}{B^2}\frac{i(\omega + |\omega_{*i}|)k_y}{k_{\parallel}}\tilde{E}_y. \tag{5A.13}$$

Substituting equation (5A.13) into Ampère's law, $\partial \tilde{B}_x/\partial y = \mu_0 \tilde{J}_z$, we have

$$\tilde{B}_x = \frac{\mu_0 m_i n_i}{B^2}\frac{(\omega + |\omega_{*i}|)}{k_{\parallel}}\tilde{E}_y = \frac{(\omega + |\omega_{*i}|)}{k_{\parallel}v_A^2}\tilde{E}_y. \tag{5A.14}$$

Combining equation (5A.14) and equation (5A.9), we have the dispersion relation as

$$\left\{\omega - \omega_* - \frac{k_{\parallel}^2 c_s^2}{\omega} + (\omega + \omega_*)k_{\perp}^2\rho_i^2\right\} = \omega\left\{\omega - \omega_* + (\omega_* - |\omega_{*i}| - \omega)\frac{k_{\parallel}^2 c_s^2}{\omega^2}\right\}\frac{(\omega + |\omega_{*i}|)}{k_{\parallel}^2 v_A^2}. \tag{5A.15}$$

Noting the relation $c_s^2 \ll v_A^2$ for the parameters of our interest, $\beta \ll 1$, the right-hand side of equation (5A.15) is simplified as

$$\frac{\omega(\omega - \omega_*)(\omega + |\omega_{*i}|)}{k_{\parallel}^2 v_A^2}.$$

If the finite-gyro-radius effect in the left-hand side of equation (5A.15) is neglected, $k_y^2\rho_i^2 \ll 1$, equation (5A.15) becomes

$$\left(\omega - \omega_* - \frac{k_{\parallel}^2 c_s^2}{\omega}\right) = \frac{\omega(\omega - \omega_*)(\omega + |\omega_{*i}|)}{k_{\parallel}^2 v_A^2}. \tag{5A.16}$$

Equation (5A.16) provides the dispersion relation for the low frequency electromagnetic modes in inhomogeneous plasmas.

The dispersion relation (5A.16) provides two approximate relations. They are expressed for the slow branch, $\omega^2 \ll k_{\parallel}^2 v_A^2$, as

$$(\omega^2 - \omega_*\omega - k_{\parallel}^2 c_s^2) \simeq 0 \tag{5A.17}$$

and for the fast branch, $\omega^2 \gg k_{\parallel}^2 c_s^2$, as

$$(\omega^2 + |\omega_{*i}|\omega - k_{\parallel}^2 v_A^2) \simeq 0. \tag{5A.18}$$

Equation (5A.17) corresponds to the drift waves, and the latter equation (5A.18) represents the drift-Alfvén waves.

Chapter 6

Low Frequency Instabilities in Confined Plasmas

In chapter 5, dispersion relations of modes are discussed. Various plasma modes can be excited by a small amount of external perturbation, if the spatio-temporal structure satisfies the dispersion relation. In inhomogeneous and nonequilibrium plasmas, modes can be spontaneously excited, and violate the symmetry of the mechanical equilibrium state. Such a mode is called instability. The propagating pattern $\exp(i\boldsymbol{k}\cdot\boldsymbol{x}-i\omega t)$ grows exponentially in time if the imaginary part of the frequency, $\omega=\omega_r+i\gamma$, is positive. Unstable modes are expected to appear at a high level in fluctuations. Owing to this reason, much work has been devoted to the linear stability analysis of various plasma modes. If one tries to account for all of the geometrical effects in an experimental setup, a variety in theoretical analyses on plasma instabilities would be seen (as was the case in the literature). Since inhomogeneity is one of the origins of plasma instability, an analysis in a complex geometry would be inevitable. However, we here try to reduce the geometrical complexity as far as possible, and choose typical examples which are relevant in confined plasmas.

6.1 Reactive Instability and Dissipative Instability

There are two typical mechanisms in inducing instability. They cause reactive instability and dissipative instability.

The equation of motion in the presence of a small amplitude perturbation could be rewritten in a study of the ion sound wave as

$$m_i n_i \frac{\partial^2}{\partial t^2}\tilde{V}_{iz} = T_e n_i \nabla^2 \tilde{V}_{iz} \tag{6.1}$$

which yields the dispersion relation $\omega^2 = c_s^2 k_\parallel^2$. By the introduction of a

displacement $\tilde{V}_{iz}=\partial\xi_z/\partial t$, the relation is rewritten as

$$m_i \frac{\partial^2}{\partial t^2}\xi_z = -T_e k_\parallel^2 \xi_z. \tag{6.2}$$

This relation means that the restoring force, $-T_e k_\parallel^2\xi_z$, works in the opposite direction to the displacement ξ_z, like a spring. A small perturbation does not grow in time but oscillates. In contrast, if the sign of the restoring force is reversed, i.e., the force is in the direction to increase the displacement, then a small perturbation grows exponentially. When there is a mechanism giving rise to a force in the direction of displacement, it is called *reactive instability*. Another type is *dissipative instability*.

As an analogy to plasma instabilities, let us study the motion of a point mass under gravity shown in figure 6.1. The surface to constrain the motion is given as

$$z = -\frac{1}{L}(x^2+y^2). \tag{6.3}$$

It is well known that a point $(x, y) = (0, 0)$ is an *unstable* equilibrium point. If the position is perturbed by the amount of ξ_x in the x-direction, the force in the x-direction is given as $F_x = 2mg\xi_x/L$, where m is the mass of the particle and g is the gravity. This force causes an exponential growth of deviation ξ_x with the growth rate

$$\gamma_0 = \sqrt{\frac{2g}{L}}. \tag{6.4}$$

This belongs to a family of reactive instability.

Consider the case where the point mass in figure 6.1 is charged (charge Q) and the system is subject to a uniform vertical magnetic field B (in the

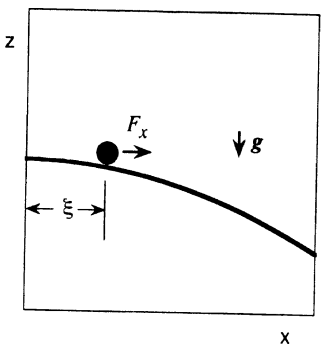

Figure 6.1. Mass point on a sliding surface.

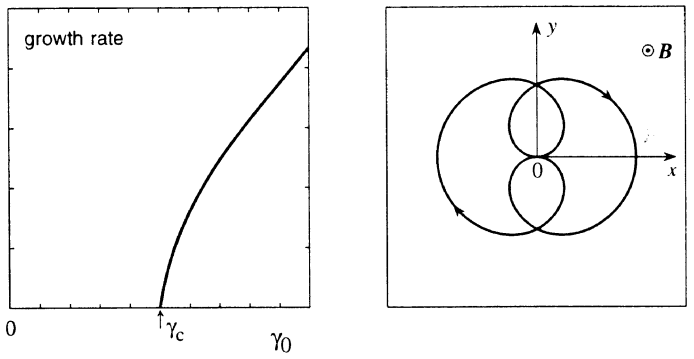

(a) (b)

Figure 6.2. Growth rate as a function of the driving parameter (a). Example of the stable orbit ($\gamma_0 < \gamma_c$) is shown in (b).

z-direction). In this situation, the Lorentz force modifies the growth rate. For temporal evolution of the type $\exp\{-i\omega t\}$, the eigenvalue ω is given as

$$\omega = \frac{\pm\left(\Omega \pm \sqrt{\Omega^2 - 4\gamma_0^2}\right)}{2} \tag{6.5}$$

where $\Omega = QB/m$. The growth rate is shown in figure 6.2(a). An example of the trajectory is presented in figure 6.2(b). There is a critical value for the driving term,

$$(g/L)_c = \Omega^2/8$$

and the system is stable in the region of

$$(g/L) < (g/L)_c \qquad \text{i.e., } \gamma_0 \leq \gamma_c = \Omega/2. \tag{6.6}$$

This system shows a feature of *dissipative* instability. If there is a friction between the point mass and the surface, the equation of motion ($v = \partial\xi/\partial t$) is written as

$$\frac{\partial}{\partial t}v = \gamma_0^2\xi + \Omega v \times \hat{z} - \nu v. \tag{6.7}$$

For the temporal evolution in the form of $\exp(-i\omega t)$, the eigenvalue ω is given as

$$\omega = \frac{-i\nu + \Omega \pm i\sqrt{4\gamma_0^2 - \Omega^2 + 2i\nu\Omega + \nu^2}}{2}. \tag{6.8}$$

Now the system turns out to be always unstable. In particular, near the marginal stability condition, $(g/L) \sim (g/L)_c$, the growth rate of perturbation is approximately given as

$$\mathrm{Im}(\omega) \cong \frac{1}{2}\sqrt{\nu\Omega}. \tag{6.9}$$

The growth rate depends on the fractional power of the dissipation rate. Even if the friction is small, $\nu/\Omega \ll 1$, its impact on the stability is prominent. This is also characteristic of the dissipative instability.

In the zero-driving limit, $\gamma_0 \to 0$, the growth rate of dissipative mode behaves as

$$\mathrm{Im}(\omega) \cong \frac{\nu\gamma_0^2}{\Omega^2}. \tag{6.10}$$

The growth rate is linearly proportional to the frictional coefficient.

In the presence of a dissipation, the gravitational energy is slightly dissipated by the friction. Hence, the velocity is reduced. The Lorentz force becomes less and is not enough to restore the orbit to the original point even in the region $(g/L) < (g/L)_c$. The point mass gradually slides down the slope, releasing the gravitational energy. This is an example of a mechanism where a dissipation can cause instability, and cause an exponential growth of the perturbation with a symmetry breaking [2.1]. The growth rate and typical trajectory are illustrated in figure 6.3.

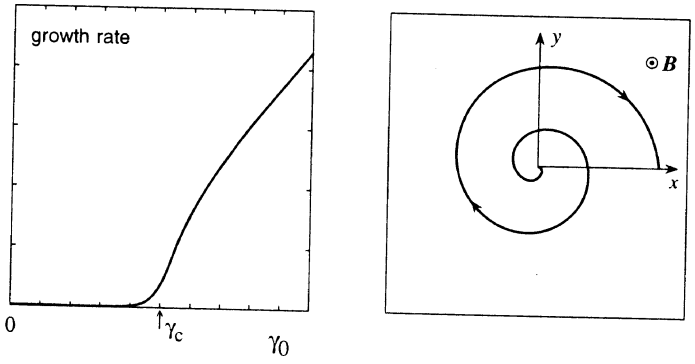

(a) (b)

Figure 6.3. Dissipative instability exists in the region of weak gradient, $\gamma_0 < \gamma_c$. Growth rate against the driving parameter (a), and a typical example of a trajectory for the case of $\gamma_0 = \gamma_c$ and $\nu \simeq \gamma_0/100$ (b).

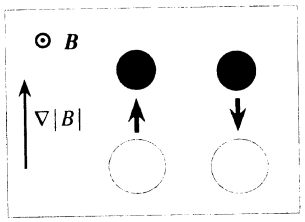

Figure 6.4. Motion of plasma in the direction of the gradient of the magnetic field. A cross-section of the plasma tube is shown. In this figure, plasma is compressed if it is moved upward, and expands when moved downward.

The dissipative instability is important from the viewpoint of nonequilibrium thermodynamics. A reactive instability usually has a larger linear growth rate; however, linear reactive instabilities could be eliminated by a proper choice of the plasma configurations [2.7–2.11]. Nonlinearities may play a dominant role in stabilizing such perturbations. In contrast, in a dissipative instability the dissipation may not be unaltered but could be *enhanced* by the development of fluctuations. If this is the case, the dissipative instability could have the nature of subcritical turbulence. This situation provides more variety in the dynamics in comparison with supercritical turbulence.

6.2 Magnetic Curvature and Pressure Gradient

An inhomogeneity of the magnetic field strength plays a role like that of the gravity in the model of figure 6.1. When plasma moves across a main magnetic field, the magnetic flux in each plasma element is approximately conserved. This nature originates from the high electrical conductivity along the magnetic field line, which is due to the approximately free electron motion. The magnetic field is often described as *frozen in* plasma [2.4, 1.6]. If this is the case, then the cross-section of the plasma element changes as it moves in the direction of the gradient of magnetic field strength. It is compressed when it moves to a high field side; it is expanded when it moves to a low field side (figure 6.4). The plasma may release the free energy when it expands. If this released energy is transformed so as to enhance a plasma displacement, as is the case of a mass point on the top of a hill, then an instability occurs. The confined state of the plasma is easily destroyed.

Owing to this nature, the influence of magnetic field inhomogeneity has long been investigated in relation to the plasma confinement. A simplest example is known as *interchange instability* [6.1]. In a real system, the curvature of the magnetic field line is not constant, and a perturbation may be localized in a particular region along the magnetic field line. In the latter case, the perturbation is called a *ballooning mode* [2.1].

6.2.1 Magnetic Well and Magnetic Hill

Consider a case where a magnetic field (mainly in the z-direction) is inhomogeneous in the x-direction. The cross-section of the x–z-plane is shown in figure 6.5, where the x-axis is taken in the direction of inhomogeneity, and the z-axis is in the direction of the strong magnetic field. The magnetic field inhomogeneity is usually induced by the curvature of the field line. The limiting case is taken as an example, where a plasma current is small and does not affect the magnitude of the magnetic field. (This condition is approximately satisfied in wide circumstances.) Ampère's law $\nabla \times \boldsymbol{B} = \mu_0 \boldsymbol{J} = 0$ provides the relation

$$B_x = \left(\frac{\partial}{\partial x} B_z\right) z \tag{6.11}$$

where the origin $z = 0$ is taken at the point where $B_x = 0$ is satisfied. The magnetic field line is expressed as, with the integration of the equation of the field line $\mathrm{d}x/B_x = \mathrm{d}z/B_z$, as

$$x = \frac{1}{2}\left(\frac{1}{B_z}\frac{\partial B_z}{\partial x}\right) z^2.$$

It is expressed by use of a curvature R_M as

$$x = \frac{1}{2R_M} z^2. \tag{6.12}$$

The curvature R_M is related to the gradient of the strength of the magnetic field as

$$\frac{1}{R_M} = \frac{1}{B_z}\frac{\mathrm{d}}{\mathrm{d}x}|B_z|. \tag{6.13}$$

The directions of both the gradients of plasma pressure and magnetic field strength are the key. An inhomogeneous and magnetized plasma, in an inhomogeneous magnetic field, is shown in figure 6.6. The (x, z)-cross-section is as shown in figure 6.5. When the plasma pressure is higher in the region where the magnetic field is stronger, as in figure 6.6(a),

$$\nabla p \cdot \nabla |B| > 0 \tag{6.14}$$

the configuration is called a *magnetic hill*. The magnetic field becomes weaker away from the plasma. In the opposite case, figure 6.6(b),

$$\nabla p \cdot \nabla |B| < 0 \tag{6.15}$$

it is called a *magnetic well*. The field becomes stronger away from the plasma. In the case of figure 6.6(a), the system has been known to become unstable.

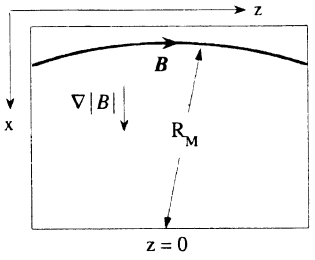

Figure 6.5. Inhomogeneity of the magnetic field. The gradient of the strength of the magnetic field is closely related to the curvature of the magnetic field line.

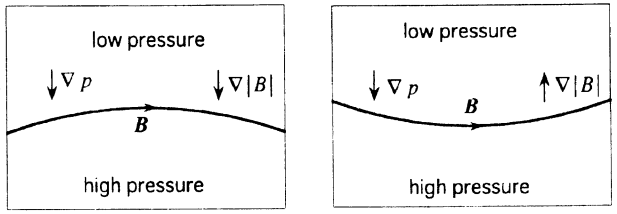

Figure 6.6. The case of a magnetic hill (unfavourable curvature, (a)) and magnetic well (favourable curvature, (b)).

6.2.2 Interchange Mode

Instabilities which appear under the configuration of a magnetic hill (figure 6.6(a)) are known by the name of interchange modes [6.1]. The growth rate is evaluated in the following.

Consider the case where a main magnetic field is in the z-direction with its gradient in the x-direction. The plasma pressure is also inhomogeneous in the x-direction (figure 6.7). This system is subject to a potential perturbation of the spatial form

$$\tilde{\phi} = \phi \exp(iky).$$

The perturbation is uniform along the magnetic field line. The consequence of this perturbation is explained in figure 6.7. The $\boldsymbol{E} \times \boldsymbol{B}$ motion appears in the x-direction. This flow causes a temporal change of density of the form

$$\tilde{n} = n_1 \exp(iky - i\pi/2).$$

A perturbed amplitude n_1 is related to the perturbed potential through the

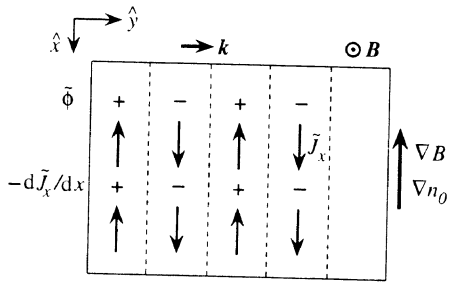

Figure 6.7. Current flow pattern (vertical arrows) associated with the potential perturbation $\tilde{\phi}$. Dotted lines denote the nodes of $\tilde{\phi}$. The magnitude of $\tilde{J}_x$ depends on x, and divergence of the perturbed diamagnetic current $\nabla \cdot \tilde{\boldsymbol{J}}$ appears. (Signs of $\tilde{\phi}$ and $-\nabla \cdot \tilde{\boldsymbol{J}}$ are denoted by + or −. They have the same sign in this case.)

continuity equation, which is written as

$$\partial \tilde{n}/\partial t = (dn_0/dx)(ik\tilde{\phi}/B)$$

when the density is inhomogeneous in the x-direction. If this density perturbation appears, a perturbation in diamagnetic current is also associated with it as

$$\tilde{J}_x = -ikB^{-1}(T_e + T_i)\tilde{n}.$$

A divergence of perturbed current remains, because the magnetic field B is inhomogeneous in the x-direction. The divergence of this diamagnetic current is given as

$$\partial \tilde{J}_x/\partial x = \frac{k^2}{B}\left(\frac{d}{dx}\frac{1}{B}\right)\frac{dn_0}{dx}(T_e + T_i)\int d\tilde{\phi}. \tag{6.16}$$

The growth rate is evaluated from this relation equation (6.16). The divergences of electric field and perturbed diamagnetic current are related as

$$\varepsilon_0\varepsilon_\perp \frac{\partial}{\partial t}\nabla_\perp \cdot \boldsymbol{E}_\perp = -\nabla \cdot \boldsymbol{J} \tag{6.17}$$

where

$$\varepsilon_\perp = c^2/v_A^2 \tag{6.18}$$

is the perpendicular dielectric constant in a magnetized plasma [2.3, 2.4]. (Notice that $\varepsilon_0(\varepsilon_\perp - 1)\partial E/\partial t$ is a polarization current in the magnetized plasma. Equation (6.17) is derived from Maxwell's equation and the charge conservation condition.) Substituting equation (6.16) into equation (6.17), one has the equation of motion,

$$\varepsilon_0\varepsilon_\perp \frac{\partial}{\partial t}(ik_y)E_y = -\frac{k^2}{B}\left(\frac{d}{dx}\frac{1}{B}\right)\frac{dn_0}{dx}(T_e + T_i)\int d\tilde{\phi}. \tag{6.19}$$

An electric field and a potential is related as $E_y = -ik_y\tilde{\phi}$. Replacing E_y by $-ik_y\tilde{\phi}$ in equation (6.19), one has

$$\varepsilon_0\varepsilon_\perp\frac{\partial^2\tilde{\phi}}{\partial t^2} = -\frac{k^2}{B}\left(\frac{\mathrm{d}}{\mathrm{d}x}\frac{1}{B}\right)\frac{\mathrm{d}n_0}{\mathrm{d}x}(T_e + T_i)\tilde{\phi}$$

or

$$\frac{\partial^2}{\partial t^2}\tilde{\phi} = \frac{c_s^2}{L_pL_M}\tilde{\phi}. \tag{6.20}$$

Here, L_p and L_M are the gradient lengths of pressure and magnetic field, respectively,

$$\frac{1}{L_p} = -\frac{\nabla p}{p} \text{ and } \frac{1}{L_M} = -\frac{\nabla B}{B}. \tag{6.21}$$

Equation (6.20) provides the growth rate γ as

$$\gamma^2 = \gamma_0^2 \equiv \frac{c_s^2}{L_pL_M}. \tag{6.22}$$

This result shows that a potential perturbation grows exponentially, if the sign of the coefficient of the right-hand side of equation (6.20) is positive, i.e.,

$$\frac{1}{L_pL_M} > 0. \tag{6.23}$$

The perturbation is unstable if a magnetic field becomes weaker in the direction in which the plasma pressure decreases. Under such a situation, a magnetic field is said to have a *bad curvature* (*unfavourable curvature*). In contrast, if the magnetic field becomes stronger as the pressure decreases, $L_pL_M < 0$, the system is stable. In this case the magnetic field has a *good* (*favourable*) curvature. As an example, one may imagine plasmas that are confined by the dipole field of the earth (or stars) (figure 6.8). If a ring of plasma is formed around the equator plane, the magnetic curvature is favourable for the inside part of the ring, and is unfavourable for the outside part.

In the case of interchange instability, it is possible to show that the force is in proportion to the displacement. The perturbed electric field is rewritten in terms of the $\boldsymbol{E}\times\boldsymbol{B}$ velocity, $\tilde{V}_x^{E\times B} = \tilde{E}_y/B = -ik_y\tilde{\phi}/B$. Then equation (6.19) is rewritten in the form of the equation of motion

$$m_in_i\frac{\partial}{\partial t}V_x^{E\times B} = \frac{m_in_ic_s^2}{L_pL_M}\xi_x^{E\times B} \equiv F_x \tag{6.24}$$

where $\xi_x^{E\times B}$ is the displacement by the $\boldsymbol{E}\times\boldsymbol{B}$ motion

$$\xi_x^{E\times B} = \int \mathrm{d}t\, V_x^{E\times B}. \tag{6.25}$$

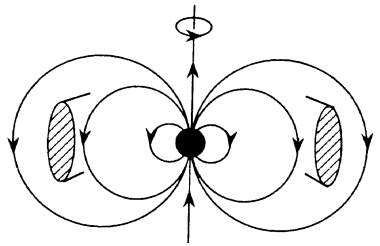

Figure 6.8. Plasma (shaded portion) confined by the dipole magnetic field of a star.

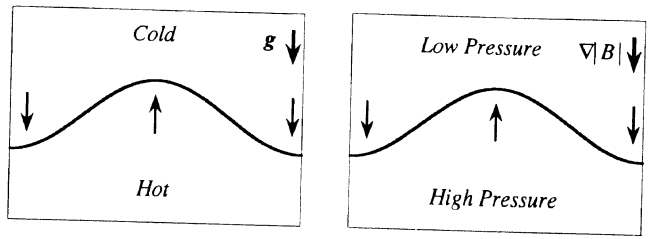

Figure 6.9. Rayleigh–Benard convection (a) and the interchange mode (b). Perturbation in the flow is shown by the arrow, and the iso-temperature (pressure) surface is also illustrated.

It is shown in equation (6.24) that the force F_x is in proportion to the displacement $\xi_x^{E\times B}$ in the x-direction. The force increases the displacement if the condition $L_pL_M > 0$ is satisfied.

This instability shows a close analogy with a Rayleigh–Taylor instability in fluid dynamics [6.2]. When water is heated from the bottom under a gravitational force, the thermal expansion causes an upward flow due to the buoyancy (figure 6.9). A convection roll is formed. In this case, the viscosity and thermal conduction tend to impede the convective motion. A roll pattern becomes unstable if the temperature gradient exceeds a threshold, which is known as a critical Rayleigh number. If water is heated from the top, the vertical temperature structure is stable. A combination of temperature gradient and gravity causes a Rayleigh–Benard convection. In a plasma, a combination of pressure gradient and effective force due to the magnetic field gradient causes an $\boldsymbol{E}\times\boldsymbol{B}$ convection.

6.2.3 Finite $k_\parallel$ Effect and Dissipative Instability

Next we consider a case where a perturbation is not uniform along a field line. In the example of section 6.2.2, no variation is introduced along the magnetic field line. In this section, it is illustrated that parallel dynamics is important for plasma instabilities.

The mode number vector has a parallel component to the magnetic field line,

$$\boldsymbol{k} = (0, k, k_\parallel)$$

and a plasma is perturbed in the x-direction as

$$\xi_x = \xi \exp(\mathrm{i}ky + \mathrm{i}k_\parallel z - \mathrm{i}\omega t).$$

In the presence of small but finite collisions, the equation of electron motion along the field line becomes $m_e \mathrm{d}\tilde{V}_{e\parallel}/\mathrm{d}t = -e\tilde{E}_\parallel - m_e\nu_{ei}\tilde{V}_{e\parallel}$. A perturbed electron current along the field line $\tilde{J}_\parallel = -n_e e\tilde{V}_{e\parallel}$ is given as

$$\tilde{J}_\parallel = \frac{n_e e^2}{m_e(\nu_{ei} - \mathrm{i}\omega)}\tilde{E}_\parallel \tag{6.26}$$

where ν_{ei} is the electron–ion collision frequency. (If one takes a stationary limit, $\omega \to 0$, this relation reduces to the usual Ohm law, $\tilde{J}_\parallel = (n_e e^2/m_e\nu_{ei})\tilde{E}_\parallel$.) By use of the relation

$$\boldsymbol{E}_\parallel = -\partial \boldsymbol{A}_\parallel/\partial t - \nabla_\parallel \phi$$

the perturbed current is expressed in terms of electrostatic potential as

$$\tilde{J}_\parallel = \left(1 + \frac{\omega}{\omega + \mathrm{i}\nu_{ei}}\frac{\omega_p^2}{k_\perp^2 c^2}\right)^{-1} \frac{n_e e^2}{m_e}\frac{k_\parallel}{(\omega + \mathrm{i}\nu_{ei})}\tilde{\phi} \tag{6.27}$$

where the relation between current and vector potential,

$$\mu_0 \tilde{J}_\parallel = k_\perp^2 \tilde{A}_\parallel \tag{6.28}$$

is used.

In this case a bending of the magnetic field line with the nodes causes an additional restoring force and reduces the growth rate. The reduction of growth rate is understood from the observation of a pattern of perturbed current (figure 6.10). Since $\tilde{J}_\parallel$ is not constant along the field line, but changes its direction within a wavelength $1/k_\parallel$, the divergence of $\tilde{J}_\parallel$ is compensated by the perpendicular current $\tilde{J}_\perp$, $\tilde{J}_\perp \simeq (k_\parallel/k_\perp)\tilde{J}_\parallel$. The Lorentz force $\tilde{J}_\perp \times \boldsymbol{B}$ is directed in the direction so as to restore the deformation in the x-direction. Its magnitude is given as

$$(\tilde{J}_\perp \times \boldsymbol{B})_\perp = \left(1 + \frac{\omega}{\omega + \mathrm{i}\nu_{ei}}\frac{\omega_p^2}{k_\perp^2 c^2}\right)^{-1} \frac{n_e e^2}{m_e}\frac{k_\parallel^2 B}{(\omega + \mathrm{i}\nu_{ei})k_\perp}\tilde{\phi}$$

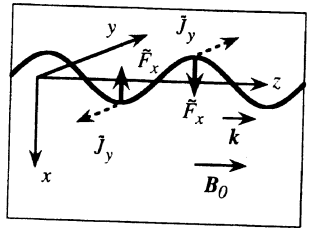

Figure 6.10. Perturbed magnetic field line and the current in the y-direction (dotted arrow). Restoring force $\tilde{F}_x$ (thick arrow) appears.

$$= \left(1 + \frac{\omega}{\omega + \mathrm{i}\nu_{ei}}\frac{\omega_p^2}{k_\perp^2 c^2}\right)^{-1} \frac{n_e e^2}{m_e}\frac{\mathrm{i}k_\parallel^2 B^2}{(\omega + \mathrm{i}\nu_{ei})k_\perp^2}\tilde{V}_x \tag{6.29}$$

where $\tilde{V}_x$ is the $\boldsymbol{E}\times\boldsymbol{B}$ velocity due to the fluctuating field, $-\mathrm{i}k\tilde{\phi}/B$. Adding this restoring force to the right-hand side of equation (6.24), the dispersion relation is now given as

$$\omega^2 + \gamma_0^2 - \left(1 + \frac{\omega}{\omega + \mathrm{i}\nu_{ei}}\frac{\omega_p^2}{k_\perp^2 c^2}\right)^{-1} \frac{\omega}{\omega + \mathrm{i}\nu_{ei}}\frac{\omega_p^2}{k_\perp^2 c^2}k_\parallel^2 v_A^2 = 0 \tag{6.30}$$

where $\gamma_0^2 = c_s^2/L_p L_M$. In the limit of $k_\parallel = 0$, it becomes equation (6.20).

We first study a limiting case of long perpendicular wavelength, i.e.,

$$\frac{\omega_p^2}{k_\perp^2 c^2} \gg 1. \tag{6.31}$$

(An opposite limit is discussed in the next subsection.) In this case, the dispersion relation equation (6.30) is simplified as

$$\omega^2 + \gamma_0^2 - \left(1 - \frac{\mathrm{i}\nu_{ei}}{\omega}\frac{k_\perp^2 c^2}{\omega_p^2}\right)k_\parallel^2 v_A^2 = 0. \tag{6.32}$$

The leading term with respect to the dissipation is retained. By use of a dc electric resistivity,

$$\eta = \mu_0 \nu_{ei} c^2 \omega_p^{-2}$$

equation (6.32) is rewritten as

$$\omega^2 + \gamma_0^2 - \left(1 - \frac{\mathrm{i}\eta k_\perp^2}{\mu_0 \omega}\right)k_\parallel^2 v_A^2 = 0. \tag{6.33}$$

Equation (6.33) predicts existences of both reactive and dissipative instabilities. A reactive instability is first explained, and a dissipative instability is discussed next.

Stabilizing effect of parallel wave number. In a collisionless limit, the dispersion relation (6.33) reduces to

$$\omega^2 + \gamma_0^2 - k_\parallel^2 v_A^2 = 0. \tag{6.34}$$

The growth rate γ is shown by the dashed line in figure 6.11. The relation (6.34) shows that there is a critical driving power γ_0^2 for a reactive instability. In the absence of electron collision, $\nu_{ei}/\omega \to 0$, equation (6.34) predicts that the mode is stable (i.e., ω is real), below a critical condition

$$\gamma_0 < |k_\parallel| v_A. \tag{6.35}$$

This result shows that the reactive instability is suppressed if the parallel mode number is large enough. Substituting the explicit form of driving term γ_0, we obtain a stability limit, equation (6.35), in the form

$$c_s/\sqrt{L_p L_M} < |k_\parallel| v_A.$$

If one introduces the ratio of sound velocity to Alfvén velocity, the stability boundary is rewritten in terms of beta value. For a plasma with singly charged ions and $T_e \simeq T_i$, the ratio of velocities is rewritten as $(c_s/v_A)^2 = \beta/2$. Equation (6.35) is read as

$$\beta < \beta_c = 2L_p L_M k_\parallel^2. \tag{6.36}$$

This relation is often referred to as a *beta limit* in plasma confinements [2.1].

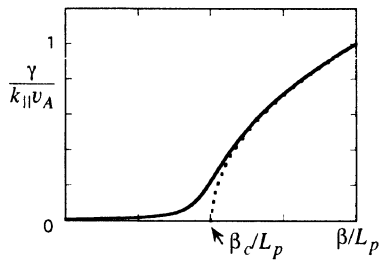

Figure 6.11. Growth rate as a function of the pressure gradient for a fixed value of $k_\parallel$. The reactive instability is shown by the dashed line. Below the critical pressure gradient, $\beta/L_p < \beta_c/L_p$, the dissipative instability remains.

The criterion (6.36) is often called the ideal MHD limit. This is based on the fact that the parallel electric field nearly vanishes, when the dispersion relation equation (6.34) is satisfied. This is seen as follows. In a limit of high density

and small electron inertia, equation (6.31), the perturbed current, equation (6.27) is simplified as

$$\boldsymbol{J}_\parallel \simeq \frac{ik_\perp^2}{\omega\mu_0}\nabla_\parallel \phi.$$

Rewriting the current, $\boldsymbol{J}_\parallel$, in terms of the vector potential $\boldsymbol{A}_\parallel$ by use of equation (6.28), this relation is equivalent to the equation

$$\boldsymbol{E}_\parallel = -\partial \boldsymbol{A}_\parallel/\partial t - \nabla\phi \simeq \boldsymbol{0}.$$

In other words, the static and inductive electric fields balance. This is because the parallel conductivity is large, so that the net parallel electric field vanishes.

Dissipative instability. A small but finite dissipation can cause an instability below the threshold condition of an ideal MHD instability, equation (6.35). A stability is obtained by a structure of perturbed current along the field line as is illustrated in figure 6.10. If this perturbed current is *impeded* by a certain mechanism, such as resistivity or current diffusion, then the resultant restoring force $\tilde{\boldsymbol{J}}_\perp \times \boldsymbol{B}$ is reduced. This becomes insufficient to provide the stability. The same situation as in figure 6.3 occurs in magnetized plasmas. When the electron collision is finite, a dissipative instability remains in the region $\gamma_0 < \gamma_c = |k_\parallel v_A|$ [6.3].

Near the marginal condition $\gamma_0 \simeq |k_\parallel| v_A$, equation (6.33) is approximated as

$$\omega^2 + \frac{i\eta k_\perp^2}{\mu_0 \omega}\gamma_0^2 = 0. \tag{6.37}$$

The eigenfrequency ω is complex, and the relevant growth rate is estimated as

$$\mathrm{Im}(\omega) \simeq \left(\frac{\eta k_\perp^2}{\mu_0}\right)^{2/3} \gamma_0^{2/3} = \nu_{ei}^{1/3}\gamma_0^{2/3}\left(\frac{k_\perp c}{\omega_p}\right)^{2/3}. \tag{6.38}$$

The dissipative mode has a growth rate which has the fractional power of a smallness parameter ν_{ei}/γ_0. A small but finite dissipation can induce an instability with a considerably large growth rate. The growth rate of a dissipative instability is drawn by the solid line in figure 6.11.

The importance of dissipation is illustrated in equation (6.38) by taking an example of the electron–ion collisions, i.e., the resistivity. Other types of dissipation, e.g., a current diffusivity [6.4] and Landau resonance [2.4], have also been found to be influential in causing various instabilities.

6.2.4 Short Wavelength Modes

In the limit which is opposite to equation (6.31),

$$\frac{\omega_p^2}{k_\perp^2 c^2} \ll 1 \tag{6.39}$$

the stability of a short wavelength limit is given. This limit is also called an electrostatic approximation. (This condition is more easily satisfied in dilute (or low pressure) plasmas. Hence, it is sometimes called a limit of dilute plasmas.) In this case, the dispersion relation (6.30) is simplified as

$$\omega^2 + \gamma_0^2 - \frac{\omega}{\omega + i\nu_{ei}} \frac{\omega_p^2}{k_\perp^2 c^2} k_\parallel^2 v_A^2 = 0. \tag{6.40}$$

Reactive instability. We first study the reactive instability. In the absence of electron collisions, $\nu_{ei}/\omega \to 0$, equation (6.40) predicts that the mode is stable (i.e., ω is real) below a critical condition

$$\gamma_0 < \gamma_c = \left| \frac{\omega_p}{k_\perp c} k_\parallel v_A \right|. \tag{6.41}$$

The stability boundary for the reactive instability is given in figure 6.12.

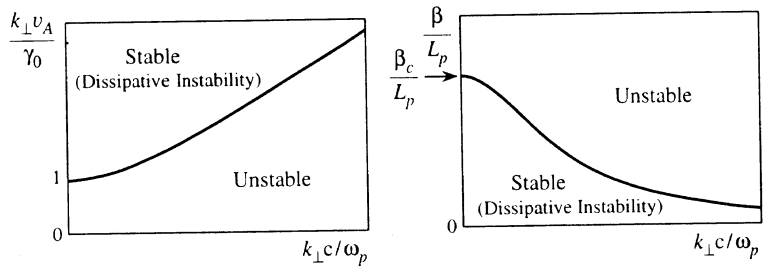

Figure 6.12. Stability boundary of the interchange mode for fixed pressure gradient (left) and for fixed $k_\parallel$ (right).

When the electron collision is finite, a dissipative instability appears in short wavelength modes. The growth rate remains in the region $\gamma_0 < \gamma_c = |k_\parallel v_A|$. Keeping the first order correction of ν_{ei}/ω, one expands the dispersion relation (6.40) as

$$\omega^2 + \left(\gamma_0^2 - \frac{\omega_p^2}{k_\perp^2 c^2} k_\parallel^2 v_A^2 \right) + \frac{i\nu_{ei}}{\omega} \frac{\omega_p^2}{k_\perp^2 c^2} k_\parallel^2 v_A^2 = 0.$$

Near the marginal condition $\gamma_0 \simeq \gamma_c = |\omega_p k_\parallel v_A / k_\perp c|$, it is approximated as

$$\omega^2 + \frac{i\nu_{ei}}{\omega} \frac{\omega_p^2}{k_\perp^2 c^2} k_\parallel^2 v_A^2 \simeq 0. \tag{6.42}$$

The growth rate is estimated as

$$\mathrm{Im}(\omega) = \nu_{ei}^{1/3} \gamma_0^{2/3}. \tag{6.43}$$

In the limit of an infinitesimally weak driving source, $\gamma_0 \to 0$, equation (6.30) provides the dispersion relation

$$\omega \simeq i\nu_{ei} \gamma_0^2 \left(\frac{k_\perp c}{k_\parallel v_A \omega_p} \right)^2. \tag{6.44}$$

(This approximate relation is derived by the help of the condition $|\omega| \ll \gamma_0$, i.e., $\gamma_0 \ll k_\parallel v_A \omega_p / k_\perp c$.) The dependence $\mathrm{Im}(\omega) \propto \nu_{ei} \gamma_0^2$ is seen to be the same as in equation (6.10).

In the short wavelength limit, there remains a reactive instability even if the condition (6.36) is satisfied. It has been considered that instabilities with short wavelength causes a gradual deterioration of confinement, and that they may not impose a drastic limit. Based on this conjecture, the condition (6.36) is considered to be a formula of a limiting plasma beta-value.

What is really important is the level to which these instabilities grow. The nature of turbulence, which is the evolution of these instabilities, is discussed in chapters 7–15.

6.2.5 Magnetic Shear

The results equations (6.35) and (6.41) indicate that the perturbation may become most dangerous if it is uniform along the field line, $k_\parallel = 0$. Efforts have been made in experimental research to eliminate the conditions which cause perturbations with $k_\parallel = 0$. One typical example is an introduction of magnetic shear as shown in figure 3.3. The expanded view is illustrated in figure 6.13. The direction of magnetic field lines inclines slightly from one magnetic surface to another. The magnetic field has the form

$$\boldsymbol{B} = \begin{pmatrix} 0 \\ \frac{x}{L_s} B \\ B \end{pmatrix} \tag{6.45}$$

in the vicinity of a mode rational surface, which corresponds to the surface $x = 0$ in equation (6.45).

In this magnetic configuration, the mode number in the direction of magnetic field is given as

$$k_\parallel = (\boldsymbol{k} \cdot \boldsymbol{B}) B^{-1} = k_y x / L_s \tag{6.46}$$

against a perturbation with the phase

$$\exp(ik_y y).$$

The magnetic field is said to have a *shear*, and L_s is called a (magnetic) shear length. The mode number along the field line, $k_\parallel$, vanishes on the surface $x = 0$, the mode rational surface. If the magnetic field has a shear, perturbation is localized in the x-direction near the surface $\boldsymbol{k} \cdot \boldsymbol{B} = 0$.

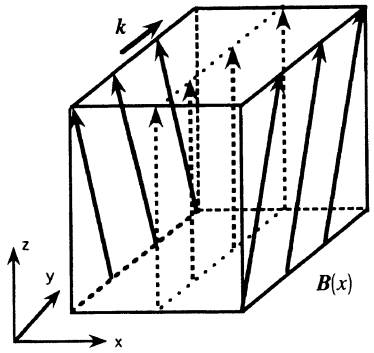

Figure 6.13. Sheared magnetic field. The dotted line indicates the mode rational surface.

In the presence of magnetic shear, the eigenvalue equation, such as equation (6.30), becomes a differential equation with respect to the variable x. This kind of procedure will be discussed at the end of this chapter.

6.2.6 Ballooning mode

The curvature of the magnetic field line is not always uniform along the field line. In the case of toroidal plasmas, the magnetic field often varies as $B \propto R^{-1}$ as is shown in figure 6.14. The curvature is bad on the outside of the torus, and is good inside. As a result of this, if one plots the driving force of the interchange mode $\nabla p \cdot \nabla B$ along the field line, it oscillates around zero with the period of $2\pi qR$. Here we simply write the variation of the curvature as a sinusoidal function as

$$c_s^2/L_pL_M = \gamma_{0M}^2\{\cos(z/2\pi qR) - h\} \tag{6.47}$$

where γ_{0M} is the peak value of the driving term, and h is a small value. A positive value of h corresponds to an average magnetic well that makes this average negative.

We take the simplest case, where the driving term is given by a sinusoidal form equation (6.47). The mode number along the field line $k_\parallel$ is replaced by the operator $-i\partial/\partial z$, and the eigenvalue equation, which is equivalent to equation (6.34), turns out to be a form of differential equation as

$$v_A^2 \frac{d^2}{dz^2}\psi(z) + \gamma_{0M}^2\{\cos(z/2\pi qR) - h\}\psi(z) + \omega^2\psi(z) = 0. \tag{6.48}$$

When c_s^2/L_pL_M is constant, $\psi(z)$ is given by a single Fourier component and the eigenvalue ω is given by equation (6.34). The solution of equation (6.48),

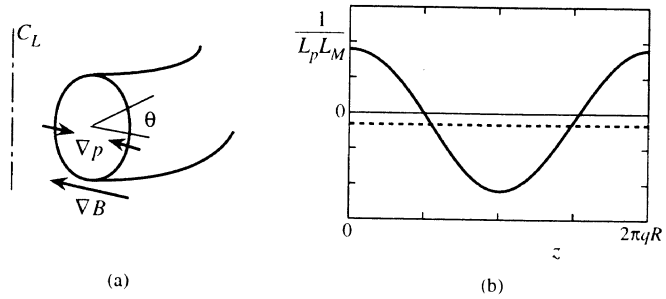

Figure 6.14. Toroidal geometry (a) and the magnetic curvature that varies along the magnetic field line (b). The average is shown by the dotted line in (b). Length z is measured along the field line in (b).

which is periodic with the period $2\pi qR$, is given by the Mathieu function

$$\psi(z) \propto ce_0(z/4\pi qR,\ 8(\pi qR/v_A)^2). \tag{6.49}$$

The eigenmode is given, in the strong drive limit, as

$$\omega^2 = -(1-h)\gamma_{0M}^2 + \frac{v_A}{2\pi qR}\gamma_{0M} \qquad \gamma_{0M} \gg v_A/2\pi qR \tag{6.50}$$

and in the weak drive limit as

$$\omega^2 = \left(h - \frac{1}{2}\left(\frac{2\pi qR}{v_A}\right)^2 \gamma_{0M}^2\right)\gamma_{0M}^2 \qquad \gamma_{0M} \ll v_A/2\pi qR. \tag{6.51}$$

The result equation (6.50) indicates that a simple estimate for the instability condition derived from equation (6.35), $\gamma_0 > k_\parallel v_A$, can be used in evaluating the region of a strong ballooning instability with the help of the estimation of $k_\parallel = 1/qR$ and the choice of the peak value $\gamma_0 \simeq \gamma_{0M}$ [2.1]. This simplification provides an estimate for the stability boundary equation (6.36) as

$$\beta < \beta_c = \frac{L_pL_M}{q^2R^2} \simeq \frac{L_p}{q^2R} \tag{6.36'}$$

where the relation $L_M \simeq R$ is used [2.1, 2.7].

The (reactive) ballooning instability disappears if

$$\gamma_{0M} \leq \sqrt{2h}\frac{v_A}{2\pi qR} \tag{6.52}$$

is satisfied. This is called stabilization by use of the *average magnetic well*.

A similar argument as for the interchange mode applies to the dissipative instability of the ballooning mode. The nonlinear dissipative ballooning mode is discussed in chapter 10. The role of the magnetic shear, which also increases $k_\parallel$, is discussed in the literature [2.8, 6.5] and is not repeated here.

6.3 Drift Instabilities

When the magnetic curvature vanishes, the interchange mode becomes marginally stable; $\gamma_0 \simeq 0$. Under such circumstances, there arises a *drift instability*, which is caused by the plasma inhomogeneity. Drift waves have been subject to special attention in the research on plasma confinement. This is because this branch of oscillation appears due to an inhomogeneity of the plasma, and can become unstable in the presence of various dissipative mechanisms.

In the absence of dissipation, this mode is purely oscillating. The mode is described by an electrostatic model. The dissipation which impedes the free motion of electrons modifies the phase relation between electron density and electrostatic potential as

$$\frac{\tilde{n}_e}{n_e} = (1 - \mathrm{i}\delta_d)\frac{e\tilde{\phi}}{T_e}. \tag{6.53}$$

Here δ_d is a small but finite numerical factor, indicating a weak delay in the electron response. This is sometimes called the delay (deviation) from the adiabatic response. As was discussed in the previous section, the ion response function is given as

$$\frac{\tilde{n}_i}{n_i} = \frac{\omega_*}{\omega}\frac{e\tilde{\phi}}{T_e}. \tag{6.54}$$

The quasineutrality condition, $\tilde{n}_e = \tilde{n}_i$, provides the dispersion relation as

$$\omega = \omega_*(1 + \mathrm{i}\delta_d) \tag{6.55}$$

showing that the delay in the electron response causes an instability if $\delta_d > 0$.

In order to see the role of the inhomogeneity in the sign of phase delay, the effect of a small number of collisions is presented as an example. When there is a small but finite friction force on electrons, $-m_e n_e \nu \tilde{v}_e$, the equation of motion of electrons is given as

$$-en_e\tilde{E}_z - \mathrm{i}k_\parallel \tilde{p}_e \cong m_e n_e \nu \tilde{v}_{ez}. \tag{6.56}$$

By use of the continuity equation, $\partial\tilde{n}/\partial t + \nabla\tilde{n}\cdot\boldsymbol{V}_d + n\nabla\cdot\tilde{\boldsymbol{V}} = 0$, the equation of the parallel electron motion yields the response function $\tilde{n}_e$. Equation (5.24) is rewritten as

$$\frac{\tilde{n}_e}{n_e} = \left(1 + \mathrm{i}\frac{\nu(\omega_* - \omega)}{k_\parallel^2 v_{the}^2}\right)^{-1}\frac{e\tilde{\phi}}{T_e} \cong \left(1 - \mathrm{i}\frac{\nu(\omega_* - \omega)}{k_\parallel^2 v_{the}^2}\right)\frac{e\tilde{\phi}}{T_e} \tag{6.57}$$

where v_{the} is the electron thermal velocity, $v_{the}^2 = T_e m_e^{-1}$. A finite delay δ_d is explicitly given as

$$\delta_d = \frac{\nu(\omega_* - \omega)}{k_\parallel^2 v_{the}^2}. \tag{6.58}$$

The necessary condition for the instability, $\delta_d > 0$, is realized if $\omega_* > \omega$ holds. In the absence of inhomogeneity, i.e., $\omega_* = 0$, δ_d is always negative. The dissipation, like electron–ion collisions, can induce a growth of fluctuations in inhomogeneous plasmas. This is the reason why the drift wave has been thought to be particularly important.

It is noticed that this kind of phase delay is caused not only by electron collisions but also by other dissipation mechanisms (e.g., electron Landau damping).

A simple estimate of drift wave dispersion, $\omega \simeq \omega_*$, predicts that the phase difference δ_d vanishes and the stability is marginal. (That is, the determination of the stability is subtle. This is one of the reasons that there is a lot of literature on the stability analysis of drift waves.) There are, however, abundant mechanisms that make the real frequency lower than the drift frequency. If the wavelength perpendicular to the magnetic field is comparable to the ion gyro-radius, the effective potential, which the ions feel, becomes smaller as is illustrated in figure 5A.1. The effective potential $\bar{\phi}$ is given as

$$\bar{\phi} = I_0(k_\perp^2\rho_i^2)\exp(-k_\perp^2\rho_i^2)\tilde{\phi} \tag{6.59}$$

where I_0 is the zeroth order modified Bessel function of the first kind. It is simplified as $(1 - k_\perp^2\rho_i^2)\tilde{\phi}$ in the limit of small finite-gyro-radius effect. The ion response is then given as

$$\frac{\tilde{n}_i}{n_i} = \frac{\omega_*}{\omega}(1 - k_\perp^2\rho_i^2)\frac{e\tilde{\phi}}{T_e} + \frac{k_\parallel^2 c_s^2}{\omega^2}\frac{e\tilde{\phi}}{T_e}. \tag{6.60}$$

The real frequency is given as

$$\omega = \omega_*\left(1 - k_\perp^2\rho_i^2 + \frac{k_\parallel^2 c_s^2}{\omega_*^2}\right) \tag{6.61}$$

and can become lower than ω_*. The growth rate is given as

$$\gamma = \frac{\nu\omega_*^2}{k_\parallel^2 v_{the}^2}\left(k_\perp^2\rho_i^2 - \frac{k_\parallel^2 c_s^2}{\omega_*^2}\right). \tag{6.62}$$

The mode is unstable for the case of $k_\perp^2\rho_i^2 > k_\parallel^2 c_s^2\omega_*^{-2}$ or

$$k_y k_\perp \rho_i^2 > k_\parallel L_n. \tag{6.63}$$

An instability is possible for smaller parallel mode number.

This instability is also influenced by the magnetic shear. There is abundant literature.

6.4 Variations

In toroidal plasmas, the geometry gives rise to variations of mode. From the physics points of view, a similarity is observed among various instabilities. Some are explained here.

6.4.1 Trapped Particle Mode

The trapped particles influence the low frequency instability [6.6]. As is discussed in chapter 3, trapped particles are localized near the low field side of the torus. The motion of the guiding centre is illustrated schematically in figure 6.15. Trapped particles do not freely move along the magnetic field lines, and they respond to the perturbed potential in a different way compared to transit particles. Due to this difference, there arise various instabilities driven by trapped particles. The number density of transit particles is given as $n_{transit} \simeq n_e(1 - \sqrt{2\varepsilon})$ and that of trapped ones is

$$n_{trap} \simeq n_e\sqrt{2\varepsilon} \tag{6.64}$$

where $\varepsilon = r/R$ is the inverse aspect ratio.

One variation is seen in a reactive instability. The response in a collisionless limit is shown. Trapped electrons are localized to a particular poloidal angle, and the parallel motion along the field line is prohibited. When a potential perturbation such as the drift wave is considered, the transit electrons move freely so as to satisfy the Boltzmann relation. In contrast, trapped particles do not move along the field line, and the response is similar to the one in the interchange mode. The perturbed density of trapped particles is expressed as

$$\frac{\tilde{n}_{trap}}{n_e} \simeq \sqrt{2\varepsilon}\frac{\omega_*}{\omega - \omega_{Mi}}\frac{e\tilde{\phi}}{T_e}. \tag{6.65}$$

The denominator $\omega - \omega_{Me}$ includes the Doppler shift owing to the toroidal drift of trapped particles, $\omega_{Me} = k_\zeta V_{De}$. A similar relation is obtained for trapped ions.

$$\frac{\tilde{n}_{trap.i}}{n_e} \simeq \sqrt{2\varepsilon}\frac{\omega_*}{\omega - \omega_{Mi}}\frac{e\tilde{\phi}}{T_e}. \tag{6.66}$$

We take a simplified case of $T_e \simeq T_i$, and use the relation $\omega_{Mi} = -\omega_{Me}$. A simple example is an extremely low frequency mode, $|k_\parallel v_{thi}| \gg \omega$ as well as $|k_\parallel v_{the}| \gg \omega$. In this circumstance, the response of transit ions is also approximated as the Boltzmann response, i.e.,

$$\frac{\tilde{n}_{transit.e}}{n_e} \simeq (1 - \sqrt{2\varepsilon})\frac{e\tilde{\phi}}{T_e} \tag{6.67}$$

$$\frac{\tilde{n}_{transit.i}}{n_e} \simeq -(1 - \sqrt{2\varepsilon})\frac{e\tilde{\phi}}{T_e}. \tag{6.68}$$

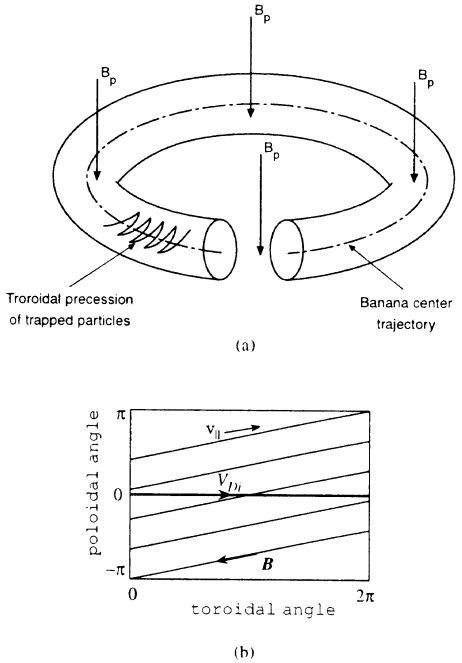

Figure 6.15. Schematic picture of the trajectory of trapped ions (a). Guiding centre motions of trapped ions (thick solid line) and untrapped ions (thin lines) are given in (b). Trapped particles move in the trough of the magnetic field, $\theta \simeq 0$, while transit particles move along the field lines.

The charge neutrality condition is rewritten as

$$2(1 - \sqrt{2\varepsilon}) + \sqrt{2\varepsilon}\frac{\omega_*}{\omega - \omega_{Me}} - \sqrt{2\varepsilon}\frac{\omega_*}{\omega + \omega_{Me}} \simeq 0. \tag{6.69}$$

The charge separation is not resolved, and a reactive instability appears as

$$\mathrm{Im}(\omega) \simeq \sqrt{\sqrt{2\varepsilon}\omega_{Me}\omega_* - \omega_{Me}^2} \simeq \varepsilon^{1/4}\sqrt{\omega_{Me}\omega_*}. \tag{6.70}$$

Like the interchange mode, this instability appears because the directions of the diamagnetic drift and the grad-B drift are in the same direction for trapped particles. The trapped particles are localized in the region where the magnetic curvature is bad.

This indicates that, if the drift direction of trapped particles is reversed, then this strong instability is suppressed. Drift reversal is possible, e.g., by

the modification of the q-profile and the shape of the cross-section, or by strong inhomogeneity of the radial electric field [6.6–6.8]. These influences are discussed later.

Trapped particles also induce a dissipative instability. In the presence of collisions, trapped electrons have a larger collision frequency compared to the transit electrons. This is because the small pitch angle scattering leads to detrapping. The effective collision frequency of trapped particles is $1/\varepsilon$ times larger than transit particles. The ratio of the number density, $n_{trap}/n_{transit} \simeq \sqrt{2\varepsilon}$, is smaller than unity. However, the collision frequency is enhanced by the factor $1/\varepsilon$, so that the contribution from trapped particles to a mode due to collisions is larger. A small but finite number of collisions for trapped particles (but neglecting those for transit particles, for simplicity) leads to the dispersion relation (6.70) as

$$2(1-\sqrt{2\varepsilon}) + \sqrt{2\varepsilon}\frac{\omega_*}{\omega-\omega_{Me}+\mathrm{i}\nu_{eff.e}} - \sqrt{2\varepsilon}\frac{\omega_*}{\omega+\omega_{Me}+\mathrm{i}\nu_{eff.i}} \simeq 0 \quad (6.71)$$

($\nu_{eff.e,i} \simeq \nu_{e,i}/\varepsilon$). Even in the absence of the effective bad magnetic curvature $\omega_{Me}\omega_* \to 0$, an instability remains. The eigenvalue is estimated as

$$\omega = -\frac{\sqrt{\varepsilon}}{2}\omega_* + \mathrm{i}\left(\frac{\varepsilon}{4}\frac{\omega_*^2}{\nu_{eff.e}} - \nu_{eff.i}\right). \quad (6.72)$$

Historically, this is called a dissipative trapped ion mode.

When the phase velocity is higher, $|k_\parallel v_{thi}| \ll \omega$, the response of transit ions deviates from the Boltzmann response. In the region of wavelength $|k_\parallel v_{thi}| \ll \omega \ll |k_\parallel v_{the}|$, the mode is the drift wave, and one must study the effect of trapped particles on the drift wave. (Figure 6.16 illustrates the regions of the trapped ion mode and trapped electron drift modes.) The drift waves $\omega \simeq \omega_*$ can be destabilized by the dissipation of trapped particles which are responding to the perturbed potential. This type of instability is called a dissipative trapped particle instability, and a lot of variations have been reported depending on the various collision frequencies.

6.4.2 Ion Temperature Gradient (ITG) Mode

The ion sound mode is destabilized by the ion temperature gradient (ITG) [6.9–6.11]. When the ion temperature is inhomogeneous in the x-direction (figure 5.1) while the density is homogeneous, the response of ions to the low frequency perturbation is calculated (figure 6.17). In this situation, the diamagnetic drift vanishes, but drift heat flow in the y-direction exists. In other words, hot ions and cold ions are moving in opposite directions in a stationary state. This instability appears due to the interactions of colder ions and hotter ions.

We consider the case

$$|k_\parallel v_{thi}| \ll \omega \ll |k_\parallel v_{the}|$$

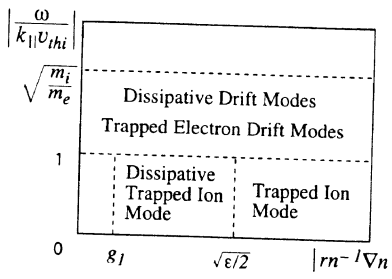

Figure 6.16. Classification of instabilities driven by density gradient. The parameter region in the density gradient and relative phase velocity is shown for the trapped ion mode and trapped electron drift modes. Criterion g_1 is given as $g_1 \sim \sqrt{\nu_{eff.e}\nu_{eff.i}\varepsilon^{-1}}rc_s^{-1}k^{-1}\rho_i^{-1}$.

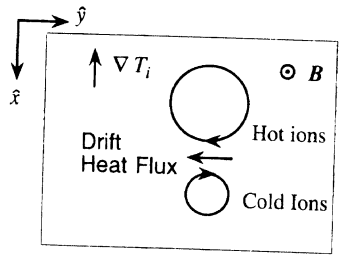

Figure 6.17. Drift heat flux in the $\nabla T \times \boldsymbol{B}$ direction appears when the plasma temperature is not uniform.

which is relevant to drift and ion sound waves. The ion response function is given in chapter 5 as $\tilde{n}_i/n_0 \cong (k_\parallel^2 c_s^2/\omega^2)(e\tilde{\phi}/T_e)$ in a homogeneous plasma. In the presence of the ITG, the ion pressure perturbation due to drift heat flow appears, and the ion response is given as

$$\frac{\tilde{n}_i}{n_0} \cong \frac{k_\parallel^2 c_s^2}{\omega^2}\left(1-\frac{\omega_{*Ti}}{\omega}\right)\frac{e\tilde{\phi}}{T_e} \quad (6.73)$$

where

$$\omega_{*Ti} = \frac{k_y}{eB}\frac{\mathrm{d}T_i}{\mathrm{d}x}. \quad (6.74)$$

The influence of the temperature gradient of ions is coupled with the parallel ion motion. The ion sound term $k_\parallel^2 v_{thi}^2/\omega^2$ is modified in the ion response. The electrons have the Boltzmann response, $\tilde{n}_e/n_0 \cong e\tilde{\phi}/T_e$, and the dispersion

relation of the ion sound wave is modified as

$$1 = \frac{k_\parallel^2 c_s^2}{\omega^2}\left(1 - \frac{\omega_{*Ti}}{\omega}\right). \tag{6.75}$$

This cubic equation in ω of equation (6.75) predicts a reactive instability for

$$\left|\frac{\omega_{*Ti}}{k_\parallel c_s}\right| \geq \frac{2}{3\sqrt{3}}. \tag{6.76}$$

The growth rate is estimated as

$$\mathrm{Im}(\omega) \simeq \omega_{*Ti}^{1/3}(k_\parallel c_s)^{2/3} \qquad \text{with } \mathrm{Re}(\omega) \simeq \omega_{*Ti}^{1/3}(k_\parallel c_s)^{2/3} \tag{6.77}$$

(for $|\omega_{*Ti}/k_\parallel c_s| \gg 1$). This instability naturally causes the mixing of hotter ions and colder ions, so that it is also called the *ion-mixing mode*. Note that (6.76) and (6.77) are valid so long as the condition $|\omega/k_\parallel v_{thi}| \gg 1$ is satisfied. The numerical factor $2/3\sqrt{3}$ in equation (6.76) should be taken as an order of magnitude estimate.

Figure 6.18 shows the growth rate and real frequency as a function of the parallel mode number. This mode becomes unstable in the long wavelength region. In the limit of large parallel mode number, $|k_\parallel|c_s \gg |\omega_{*Ti}|$, the dispersion relation equation (6.75) reduces to that of the ion sound mode.

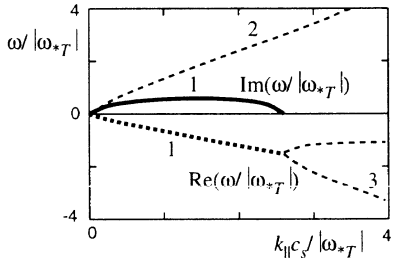

Figure 6.18. ITG mode (branch 1). Growth rate (solid line) and real frequency (dashed line) are shown. Branches 2 and 3 indicate the ion sound wave. The stable branch is shown by the thin dashed lines.

The density gradient is known to stabilize the ITG mode. The stability boundary, which is determined by the competition between density gradient and ion temperature gradient, is explained. In order to avoid the limitation $|\omega/k_\parallel v_{thi}| \gg 1$, a result based on the kinetic theory is used for the dispersion relation as [6.9]

$$1 = -\frac{T_e}{T_i}(1 + y_i Z(y_i)) - y_i Z(y_i)\frac{\omega_*}{\omega} + \frac{T_e}{T_i}\left\{y_i^2 + \left(y_i^3 - \frac{y_i}{2}\right)Z(y_i)\right\}\frac{\omega_{*Ti}}{\omega} \tag{6.78}$$

where $y_i = \omega/\sqrt{2}|k_\parallel|v_{thi}$ and $Z(y_i)$ is the plasma dispersion function. In deriving equation (6.78), the electron response is assumed to be the Boltzmann response. In the limit of $|\omega/k_\parallel v_{thi}| \gg 1$, an asymptotic relation $y_i Z(y_i) \simeq -1 - y_i^{-2}/2 - 3y_i^{-4}/4$ holds, and equation (6.78) is simplified as

$$1 = \frac{k_\parallel^2 T_e}{\omega^2 m_i}\left(1 - \frac{\omega_{*Ti}}{\omega}\right) + \frac{\omega_*}{\omega}. \tag{6.79}$$

In the absence of the temperature inhomogeneity, $\omega_{*Ti} \to 0$, this relation reproduces the one for drift waves. If one takes $\omega_* \to 0$, equation (6.75) is reproduced.

The marginal stability condition is derived from equation (6.78). When the mode is marginally stable, ω is real. The plasma dispersion function Z has a imaginary part. Therefore, at the marginal stability condition, the coefficient of the Z function and other terms must vanish, i.e., $T_e/T_i + \omega_*/\omega - (T_e/T_i)(y_i^2 - \frac{1}{2})\omega_{*Ti}/\omega = 0$ and $1 + T_e/T_i - (T_e/T_i)y_i^2\omega_{*Ti}/\omega = 0$. The real frequency and parallel wave number at the stability criterion are given as

$$\omega = \omega_* + \frac{T_e}{2T_i}\omega_{*Ti} \tag{6.80}$$

$$\frac{k_\parallel^2 v_{thi}^2}{\omega_{*Ti}^2} = \frac{T_e^2}{2T_i(T_i + T_e)}\left(\frac{1}{2} - \frac{1}{\eta_i}\right) \tag{6.81}$$

where

$$\eta_i \equiv \left(T_i^{-1}\frac{\mathrm{d}T_i}{\mathrm{d}x}\right)\left(n_i^{-1}\frac{\mathrm{d}n_i}{\mathrm{d}x}\right)^{-1}. \tag{6.82}$$

The critical condition (6.81) is shown in figure 6.19.

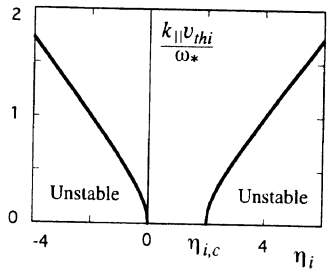

Figure 6.19. Stability/instability region for the ITG mode in the presence of the density gradient (case of $T_e = T_i$). Above the boundaries, instability is possible due to dissipation of electrons.

When the density and temperature have the gradient in the same direction, i.e., $\omega_* \omega_{*Ti} < 0$, the density gradient tends to stabilize this mode. When the ratio between the two gradients exceeds the criterion

$$\eta_i > \eta_{i,c} \tag{6.83}$$

the mode becomes unstable. The critical value $\eta_{i,c}$ satisfies $\eta_{i,c} = 2$ in the case of equation (6.78) and is of the order of unity. It has been calculated under various circumstances. (In the absence of density gradient, $\eta \to \infty$, equation (6.81) gives the stability boundary $|k_\parallel c_s/\omega_{*Ti}| = 1/2$. Comparing with this result, the analysis of the simplified fluid approximation, equation (6.76), shows a qualitative agreement.)

Even when the dispersion relation (6.78) predicts stability, there can remain a residual instability if one takes additional effects such as the finite-ion-gyro-radius effect or dissipation of electrons.

6.4.3 Toroidal ITG Mode

A cooperative effect of toroidicity and ITG causes a strong instability, which is called the toroidal ITG mode (or toroidal η_i mode) [6.11]. A simplified dispersion relation is given as

$$\frac{k_\parallel^2 c_s^2}{\omega^2} - \frac{\omega}{\omega - \omega_{*Ti}} + \frac{\bar{\omega}_{Mi}}{\omega} = 0. \tag{6.84}$$

(See [6.12] for details of derivation.) In equation (6.84), $\bar{\omega}_{Mi}$ is the Doppler shift due to the ∇B-drift of ions, $\bar{\omega}_{Mi} = k_\zeta \overline{V_{Di}}$, and the over-bar indicates an average of ∇B-drift over the region where the perturbation extends in the poloidal direction. In the absence of this Doppler shift, $\bar{\omega}_{Mi} \to 0$, equation (6.84) reduces to equation (6.75). In order to see the combined effect of the ion temperature gradient and ∇B-drift, let us take the limit of $k_\parallel \to 0$. In this limit, where equation (6.75) provides a zero growth rate, equation (6.84) yields an instability with the growth rate

$$\gamma \sim \sqrt{\omega_{*Ti} \bar{\omega}_{Mi}}. \tag{6.85}$$

The growth rate is positive if the direction of the ∇B drift of ions is the same as the ion drift heat flux (figure 6.17). This unfavourable magnetic drift appears when the magnetic curvature is bad. Stressing the importance of the bad toroidal curvature, the instability in this limit is called the toroidal ITG mode (toroidal η_i mode). The case in section 6.4.2 is called the slab ITG mode (slab η_i mode) for distinction.

In sections 6.4.2 and 6.4.3, the instability of ITG mode is derived based on an assumption of adiabatic response of electrons, i.e., $\tilde{n}_e/n_e = e\tilde{\phi}/T$. This implies that the flow of electrons is not caused by the development of ITG modes. The ITG modes, in these simple limits, do not cause particle flux, but induce selective loss of ion energy. Aiming at the explanation of anomalous ion energy flux, a lot of work has been done on the ITG modes [4.15, 6.11].

It should also be noted that the naming of the instability mode might not be the one and only possibility. In reality, several destabilizing mechanisms coexist simultaneously; one can study, e.g., destabilization of the ITG mode by trapped electrons. In such situations, the labelling of an instability by a particular name may not be unique.

6.5 Magnetic Shear and Nonlocal Mode

An introduction of the magnetic shear increases the parallel mode number, and is useful in eliminating the instability. In the case of a simplified geometry such as equation (6.45), the parallel mode number varies in the x-direction as equation (6.46),

$$k_\parallel = (\boldsymbol{k} \cdot \boldsymbol{B}) B^{-1} = k_y x / L_s$$

where $x = 0$ corresponds to the mode rational surface, $k_\parallel = 0$. In a sheared magnetic field, it is necessary to study the eigenmode structure.

An example is chosen from drift waves [6.13]. Equation (6.61) is written as

$$\left(1 - \frac{\omega}{\omega_*} + \rho_i^2 \nabla_\perp^2 + \frac{k_\parallel^2 c_s^2}{\omega_*^2}\right) \tilde{\phi} = 0 \tag{6.86}$$

where $\tilde{\phi}$ is a static potential and $\mathrm{i}k_\perp$ is replaced by $\nabla_\perp$. It is noted that $k_z = 0$ is chosen, i.e., the mode rational surface is placed at $x = 0$. The perturbation is Fourier decomposed in the y-direction. We write

$$\tilde{\phi}(x, y, t) = \phi(x) \exp(\mathrm{i}k_y y - \mathrm{i}\omega t). \tag{6.87}$$

The eigenmode equation (6.86) is rewritten, with the help of equation (6.46) $k_\parallel = k_y x / L_s$, as a differential equation

$$\left(\rho_s^2 \frac{\mathrm{d}^2}{\mathrm{d}x^2} + 1 - \frac{\omega}{\omega_*} - k_y^2 \rho_s^2 + \frac{k_y^2 c_s^2}{\omega^2 L_s^2} x^2\right) \phi(x) = 0. \tag{6.88}$$

Owing to the dependence of $k_\parallel$ on x, the nabla-operator is no longer commutable with $k_\parallel$. The sinusoidal function $\exp(\mathrm{i}k_x x)$ no longer satisfies the dispersion relation.

Equation (6.88) must be solved as an eigenvalue equation. In a dimensionless form, $x/\rho_s \to \hat{x}$, equation (6.88) is written in the form of a Weber type equation

$$\left(\frac{\mathrm{d}^2}{\mathrm{d}\hat{x}^2} + H + \sigma^2 \hat{x}^2\right) \phi(\hat{x}) = 0 \tag{6.89}$$

with the eigenvalue

$$H = 1 - \frac{\omega}{\omega_*} - k_y^2 \rho_s^2. \tag{6.90}$$

The magnitude of the magnetic shear is represented by the parameter

$$\sigma^2 = \frac{k_y^2 c_s^2}{\omega^2} \frac{\rho_s^2}{L_s^2}. \tag{6.91}$$

Equation (6.89) is solved with a proper boundary condition. The boundary condition is chosen such that the amplitude vanishes at $|\hat{x}| \to \infty$ when the mode is growing in time. (For the damped mode, the analytic continuation is used.) The eigenfunction of equation (6.89) is given as

$$\phi(\hat{x}) = \exp\left(-\frac{i\sigma^2}{4}\hat{x}^2\right) \tag{6.92}$$

with the eigenvalue

$$H = i\sigma. \tag{6.93}$$

Solving equations (6.90) and (6.93), one has the expression for the frequency.

$$\omega = (1 - k_y^2 \rho_s^2)\omega_* - i\frac{k_y c_s \rho_s}{L_s} = \left(1 - k_y^2 \rho_s^2 - i\frac{L_n}{L_s}\right)\omega_*. \tag{6.94}$$

In deriving the imaginary part of equation (6.94), σ is evaluated by use of the relation $\omega \simeq \omega_*$.

The dispersion relation (6.94) now shows a weak but finite damping rate associated with the magnetic shear. This damping rate has a relation to the sign of group velocity in the x-direction, equation (6.92). The eigenmode structure, illustrated in figure 6.20, shows that the wave energy is convected to the region $|\hat{x}| \to \infty$. The rate of energy propagating out is in proportion to the shear parameter $1/L_s$. (In the far distance, where the condition $|k_\parallel| v_{thi} \simeq \omega$ holds,

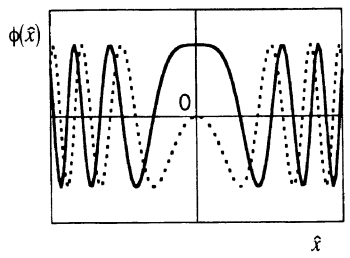

Figure 6.20. Eigenmode structure of the drift wave in a sheared magnetic field.

i.e., $|x| \simeq \rho_s L_s / L_n$, the ion Landau damping works and absorbs the wave energy [2.4].)

Comparing the eigenvalue equation (6.94) with that of a local estimate, equation (6.61), one sees that the influence of magnetic shear on the growth rate is very subtle, and careful analysis is required. The magnetic shear can also influence the phase difference of electron response [6.14]. There is plenty of literature on the linear drift instability in a sheared magnetic field [4.10, 6.15].

The propagation of the wave energy across the magnetic surface, i.e., the convective damping, is one of the principal effects of the magnetic shear. The exchange of the wave energy between particles takes place in different locations. The communication between different magnetic surfaces occurs. The nonlocal transport of the wave energy is important in analysing the turbulence-driven viscosity and related phenomena.

REFERENCES

[6.1] Rosenbluth M N and Longmire C L 1957 *Ann. Phys., NY* **1** 120
[6.2] Landau L D and Lifshitz E M 1987 *Fluid Mechanics* 2nd edn, transl. J B Sykes *et al* (Oxford: Pergamon) section 56
[6.3] Johnson J L, Greene J M and Coppi B 1963 *Phys. Fluids* **6** 1169
Johnson J L and Greene J M 1967 *Plasma Phys.* **9** 611
[6.4] Schmidt J and Yoshikawa S 1971 *Phys. Rev. Lett.* **26** 753
Kaw P J, Valeo E J and Rutherford P H 1979 *Phys. Rev. Lett.* **43** 1398
[6.5] Connor J W, Hastie R J and Taylor J B 1979 *Proc. R. Soc.* A **365** 1
[6.6] Kadomtsev B B and Pogutse O P 1971 *Nucl. Fusion* **11** 67
[6.7] Glasser A, Frieman E A and Yoshikawa S 1974 *Phys. Fluids* **17** 181
[6.8] Itoh S-I and Itoh K 1990 *J. Phys. Soc. Japan* **59** 3815
[6.9] Galeev A A, Oraevskii V N and Sagdeev R Z 1963 *Zh. Eksp. Teor. Fiz.* **44** 903 (Engl. transl. *Sov. Phys.–JETP* **17** 615)
[6.10] Coppi B, Furth H P, Rosenbluth M N and Sagdeev R Z 1966 *Phys. Rev. Lett.* **17** 377
[6.11] Further progress of analyses on the ion temperature gradient mode is surveyed in [4.15] and is seen in, e.g.,
Horton W, Estes R D and Biskamp D 1980 *Plasma Phys.* **22** 663
Waltz R E 1986 *Phys. Fluids* **29** 3684
Rewoldt G, Tang W M and Hastie R J 1987 *Phys. Fluids* **30** 807
Romaneli F 1989 *Phys. Fluids* B **1** 1018
Kotschenreuther M, Berk H L, Lebrun M J *et al* 1993 *Plasma Physics and Controlled Nuclear Fusion Research 1992* vol 2 (Vienna: IAEA) p 11
Waltz R E, Kerbel G D and Milovich J 1994 *Phys. Plasmas* **1** 2229
Kishimoto Y, Tajima T, Horton W, Lebrun M J and Kim J Y 1996 *Phys. Plasmas* **3** 1289
[6.12] Horton W Jr, Choi D-I and Tang W M 1981 *Phys. Fluids* **24** 1077
[6.13] Pearlstein L D and Berk H L 1969 *Phys. Rev. Lett.* **23** 220
[6.14] Ross D W and Mahajan S M 1978 *Phys. Rev. Lett.* **40** 324
Tsang K T, Catto P J, Whitson J C and Smith J 1978 *Phys. Rev. Lett.* **40** 327
[6.15] Tang W M 1978 *Nucl. Fusion* **18** 1089